Review of Grain Refinement of Cast Metals Through Inoculation: Theories and Developments

ZHILIN LIU

The inoculation method of grain refinement is widely used in research and industry. Because of its commercial and engineering importance, extensive research on the mechanisms/theories of grain refinement and development of effective grain refiners for diverse cast metals/alloys has been conducted. In 1999, Easton and St. John reviewed the mechanisms of grain refinement of cast Al alloys. Since then, grain refinement in alloys of Al, Mg, Fe, Ti, Cu, and Zn has evolved a lot. However, there is still no full consensus on the mechanisms/theories of grain refinement. Moreover, some new grain refiners developed based on the theories do not ensure efficient grain refinement. Thus, the factors that contribute to grain refinement are still not fully understood. Clarification of the prerequisite issues that occur in grain refinement is required using recent theories. This review covers multiple metals/alloys and developments in grain refinement from the last twenty years. The characteristics of effective grain refiners are considered from four perspectives: effective particle/matrix wetting configuration, sufficiently powerful segregating elements, preferential crystallographic matching, and geometrical features of effective nucleants. Then, recent mechanisms/theories on the grain refinement of cast metals/alloys are reviewed, including the peritectic-related, hypernucleation, inert nucleant, and constitutional supercooling-driven theories. Further, developments of deterministic and probabilistic modeling and nucleation crystallography in the grain refinement of cast metals are reviewed. Finally, the latest progress in the grain refinement of cast Zn and its alloys is described, and future work on grain refinement is summarized.

DOI: 10.1007/s11661-017-4275-7

I. INTRODUCTION

GRAIN refinement has been widely used in research and industry to achieve uniformly distributed equiaxed (or near-equiaxed) grain structures.[1,2] Not only does grain refinement have positive influences on microstructural refinement and castability (*i.e.*, the columnar-to-equiaxed transition), but it also improves the mechanical properties (*i.e.*, ductility and strength) of cast/wrought metallic materials.[3] Although some other technologies, like alloying manipulation and work hardening, can improve strength to some extent, two major safety parameters for engineering alloys, toughness and ductility, usually have to be partially sacrificed.

Research on grain refinement of cast metals has been conducted for over sixty years.[4] Grain refinement can be achieved through controlling solidification and/or solid-state processes. The two most common methods to refine the grains of cast metals are dynamic nucleation[5] and inoculation.[1] Through fast cooling and localized convection, the former can produce numerous secondary nuclei. The latter, which is extensively practiced in industry, achieves grain refinement through adding efficient grain refiners into the metal melt. When a critical undercooling is achieved, the potential nucleant particles will induce grain refinement by enhanced heterogeneous nucleation.[6–8] These nucleant particles may be released from grain refiners or form *in situ* during solidification.[9–12] Easton and StJohn[13] reviewed the mechanisms of grain refinement. They divided the theoretical and experimental reports before 1999 into two categories, the "nucleant paradigm" and "solute paradigm." Based on their review, they concluded that both effective nucleants and solute elements are required for grain refinement of Al alloys, followed by experimental validation. However, their review paper only focused on cast Al alloys. Over the last two decades, breakthroughs have been realized in the grain refinement of Al, Mg, Fe, Ti, Cu, Zn, and their alloys. The latest theories and developments need to be evaluated by reviewing recently published studies.

ZHILIN LIU is with the College of Mechanical and Electrical Engineering, Central South University, Changsha, 410083, P.R. China, and with the IMDEA Materials Institute, C/Eric Kandel 2, 28906, Getafe, Madrid, Spain, and also with the School of Mechanical and Mining Engineering, The University of Queensland, Brisbane, QLD, 4072, Australia, Contact e-mail: zhilin.liu@csu.edu.cn

Manuscript submitted September 19, 2016.
Article published online August 11, 2017

The inoculation method of grain refinement is critically reviewed here. First, the characteristics of effective grain refiners are summarized in Section II from four aspects: wetting configuration, segregating elements, crystallographic matching, and geometrical features. Then, the fundamental knowledge of nucleation and growth during grain refinement is briefly categorized in Section III. Section IV summarizes the current theories of grain refinement of cast metals, including the peritectic-related, hypernucleation, inert nucleant, and constitutional supercooling (CS)-driven theories. In Section V, recent developments in the modeling of grain refinement for cast metals are classified and critiqued. The nucleation crystallography of grain refinement is precisely reviewed for the first time in Section VI. The current grain refining theories/models have mainly been developed based on Al and/or Mg metals/alloys. Whether such theories/models can be directly applied to other non-ferrous metals, such as Zn, remains an open question. Thus, the latest progress in the grain refinement of cast Zn and its alloys is reviewed in Section VII. The review concludes with Section VIII, which describes the prerequisite criteria to design efficient grain refiners, followed by directions for future work.

II. CHARACTERISTICS OF EFFECTIVE GRAIN REFINERS

A. *Effective Particle-Matrix Wetting Configuration*

The wetting of grain refiners by liquid metal involves physical chemistry, statistical physics, long-range forces, and fluid dynamics,[14] and influences the nucleation of matrix metal grains. In a grain-refining system, a favorable wetting configuration between the liquid, particles, and grains (see Figure 1) is essential because it enables catalytic stimulation to obtain heterogeneous nucleation. In a steady state, the balance of forces imposed at a liquid–particle–grain triple conjunction should satisfy $\gamma_{nl}\cos\theta + \gamma_{sn} - \gamma_{sl} = 0$, in which γ_{nl}, γ_{sn}, and γ_{sl} denote the interfacial energy between liquid and grain, the interfacial energy between grain and particle, and the interfacial energy between liquid and particle, respectively.[15] If the wetting angle is too large, the catalytic efficiency is lowered. A strong positive

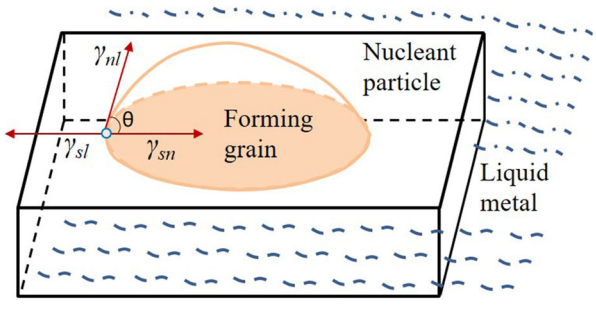

Fig. 1—Illustration of the wetting configuration between liquid metal, nucleant particle and forming grain in a grain-refining system.

interaction between a wetted particle and a forming grain may produce a small particle–grain contact angle.[16] Strong reaction and dissolution could occur when the wetting angle is close to zero.[16] However, this situation would shorten the active lifetime of the particle. To decrease the total interfacial energy between particle and grain, a favorable wetting configuration needs to satisfy $\gamma_{sl} > \gamma_{sn}$. A nucleation event can be catalyzed when the bonding of the grain matches well with that of the particle, because such matching counteracts γ_{sn}.[15,16] Normally, metal melts do not effectively wet and nucleate on particles with covalent or ionic bonding.[16] However, it has recently been reported that Mg grains nucleated on ionic MgO particles.[17]

B. *Sufficiently Powerful Segregating Elements*

Because of non-equilibrium solidification, solute segregation always unavoidably occurs during casting. Johnsson[18] was probably the first to systematically interpret the effect of solute on grain refinement. Besides nucleant particles, segregating elements are also critical to achieve grain refinement. Only specific solutes can induce remarkable grain refinement; others may have a marginal effect.[13] Solute segregation contributes to grain refinement in two ways. One is CS, which provides an additional thermodynamic driving force for new nucleation in the CS zone.[19] The other is the segregating solute in front of the solid/liquid (S/L) interface, which restricts growth of the previously formed grains.[2,13] However, Johnsson did not reveal how the nucleant particles were selected and activated. The effects of solute on grain refinement are quantified using the growth restriction factor (Q), $Q = \sum_i m_i c_{o,i}(k_i - 1)$, where m_i, $c_{o,i}$, and k_i represent the slope of the liquidus, the initial concentration of each element (assumed to be i elements in total), and the partition coefficient, respectively.[20] Figure 2 indicates that at low solute concentration, the as-cast microstructure is thermally controlled columnar grains. As the solute concentration increases, the thermal-controlled columnar growth will transition into diffusion-controlled equiaxed growth. Further increasing the solute concentration decreases the dendrite tip radius. When the dendrite tip radius eventually decreases to a critical value, the capillary effect gradually begins to dominate and then the growth rate increases, which may impair growth of equiaxed grains.[20] This phenomenon, in terms of the effects of solute on grain refinement, agrees well with the work by Kurz and Fisher[21] and Rappaz.[22] The effects of solutes on grain refinement of cast Al,[23] Mg,[24] Ti,[25] Cu,[26] and Zn[27] have been investigated. The most powerful segregating elements in liquid Al, Mg, Ti, Cu, Fe, and Zn were determined to be Ti, Zr, B, Ag/La, Cu, and Ag, respectively. These results provide some insights to design new grain refiners.

C. *Preferential Crystallographic Matching*

Lattice mismatch (or misfit) usually occurs between a matrix grain and a nucleant particle, leading to

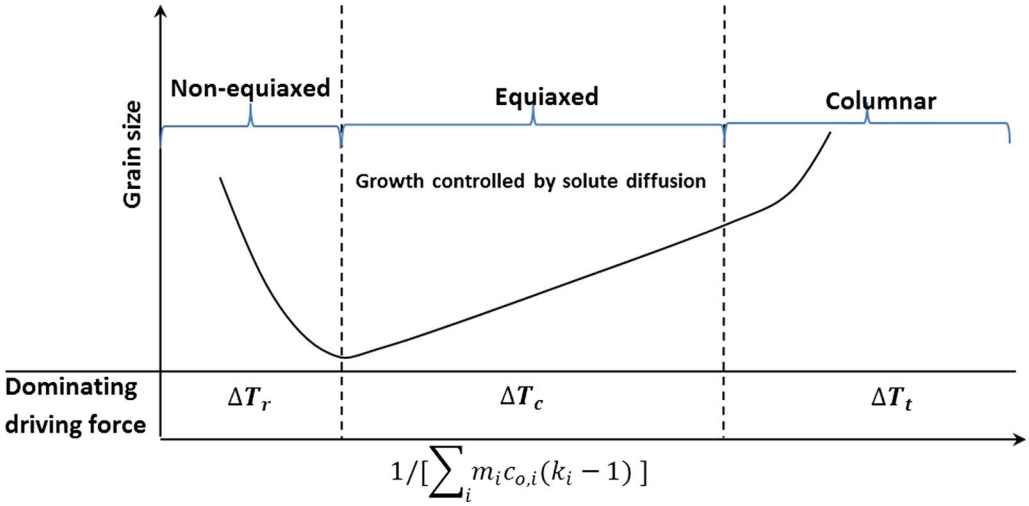

Fig. 2—Schematic graph showing how the constitutional range affects grain growth. The solute concentration decreases from right to left in the figure. (Reprinted with permission from Ref. [20]).

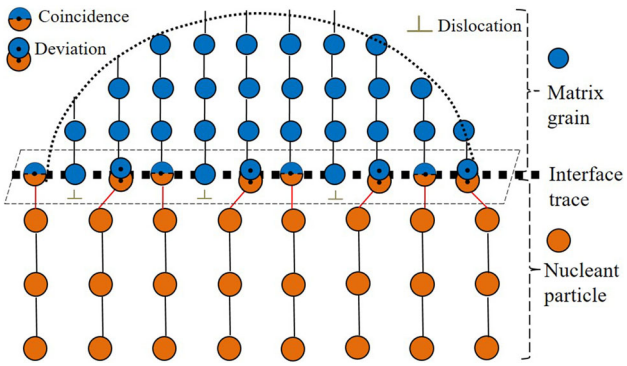

Fig. 3—The matrix grain nucleating on a nucleant particle, showing some lattice misfit between them. Both matrix and particle have crystalline structures.

dislocation at the interface between the matrix and particle, as indicated in Figure 3. If no reaction occurs at their interface, both the matrix and particle will stably preserve their individual lattice structures.[28] If the dislocation is quite small, the matrix lattice is then able to coherently match with the particle lattice through interatomic bonding. This process is termed elastic strain. Unfortunately, the presence of elastic strain may induce an energy barrier that must be overcome during nucleation. Therefore, a low lattice mismatch between matrix and particle can improve nucleation. Glicksman and Childs[29] found that (a) lattice matching affects nucleation catalysis, and (b) metallic substrates are more potent than non-metallic substrates. The term ''potency'' is used to describe the nucleation capacity of a particle serving as a nucleation site. Similarly, the studies on ductile iron by Skaland[30] revealed that the potency of a nucleant particle to induce grain refinement depends on the lattice mismatch between matrix and particle. Marcantonio *et al.*[31] found that nucleation undercooling rises with increasing lattice mismatch. Bramfitt's systematic study on the nucleation of undercooled liquid iron on nitride and/or carbide particles showed that the potency of particles is also associated with the lattice mismatch between the particle and iron matrix.[32] In many other systems investigated during solidification, the mismatch from phase A to phase B is larger/smaller than that from phase B to phase A, because nucleation seems to be unidirectional.[33] All of these studies indicate that the crystallographic matching strongly influences the nucleation in grain refinement. There are three major geometrical models used to quantify crystallographic matching including Turnbull's linear disregistry model,[34] Bramfitt's plane-on-plane disregistry model[32] and Zhang's edge-to-edge matching (E2EM) model.[7] Based on the theories of crystallographic matching, many new grain refiners have been theoretically predicted and experimentally verified.[35,36]

D. *Geometrical Features of Effective Nucleants*

The geometrical features of effective nucleant particles usually include particle size, size distribution, and morphology. The model developed by Maxwell and Hellawell[37] to explain grain refinement in Al-based peritectic alloys shows that only some of the nucleant particles (present in melts) become activated. This is attributed to (a) the latent heat released from surrounding growing grains and (b) the geometrical features of nucleant particles, which counteract the undercooling for initiation of other grains.[6,37,38] The free growth model developed by Greer *et al.*[1,39] is a breakthrough towards understanding this issue. In the free growth model, $\Delta T_{fg} = 4\sigma / \Delta S_v d$, where ΔT_{fg}, σ, ΔS_v, and d represent the free growth undercooling, S/L interfacial energy, fusion entropy, and particle size, respectively[39] (see Figure 4(a)). When ΔT_{fg} is larger than the critical undercooling for nucleation, new grains begin to initiate and grow at a steady state. Regarding the effect of particle size on grain refinement, Greer *et al.*[1,6] (Figure 4(b)), Qian *et al.*[40] and Qiu *et al.*[11] suggested that the size ranges of effective nucleant particles are 3 to 5 μm in Al/TiB_2, 1 to 5 μm in Mg/Zr, and 6 to 6.5 μm in

Mg/Al_2Y nucleating systems, respectively. Meanwhile, it has been well documented that only 1 to 2 pct of all the potential nucleant particles contribute to refining Al[39,41] and Mg alloys.[11] This percentage remains almost constant even when the amount of particles in a melt increases. Even increasing the cooling rate only increases this value up to ~4 pct.[42] However, this point may be controversial thermodynamically, because some nanoscale nucleant particles (5 to 20 nm) were recently reported to act as heterogeneous nucleation sites.[43] Additionally, Lazaridis *et al.*[44] developed a model for nucleant particles with non-uniform morphology, which predicted that the conventional uniform model underestimates the nucleation rate by several orders of magnitude. For the effective nucleant particles observed in Al, Mg, and Zn alloys, their reported morphologies vary considerably, including facet,[45] disk/needle,[46] spherical,[47] and dendrite[48] morphologies.

III. NUCLEATION AND GROWTH IN GRAIN REFINEMENT

The transformation of a metal or alloy between crystalline and non-crystalline states can be achieved through solidification. Grain nucleation and growth, which govern the kinetics of many phase transformations,[49] are the fundamental processes of solidification in grain refinement.[2] The grain sizes depend on the competition between initial nucleation and subsequent growth.[2] Classical nucleation theory[50] indicates that the Gibbs free energy difference (ΔG) for a phase transformation is approximated by

$$\Delta G = -V\Delta G_v + A\gamma + V\Delta G_s \quad [1]$$

$-V\Delta G_v$, $A\gamma$, and $V\Delta G_s$ are associated with the volume of the new phase, the surface of the new phase, and the strain energy resulting from volume misfit, respectively. The decrease of bulk ΔG is the intrinsic thermodynamic driving force for nucleation in grain refinement. It has been recognized for Al,[23] Mg,[24,36] Fe,[51] Ti,[25,52] Cu,[26] and Zn castings[27,48] that both effective particles and segregating solutes are essential for grain refinement. Actually, these two factors are closely related to nucleation and/or growth, leading to an increase in $|\Delta G|$ (or driving force). This section addresses the nucleation and growth in grain refinement from the aspects of (a) particle-enhanced grain nucleation, and (b) grain growth and CS.

A. *Particle-Enhanced Grain Nucleation*

Homogeneous nucleation and heterogeneous nucleation coexist in the solidification process of cast metals, while heterogeneous nucleation generally dominates in grain refinement. In heterogeneous nucleation, substrates (particles, impurities, surfaces) are involved when solid grains form from metal melts. This paper concentrates on particles. There are two types of nucleant particles that can act as nucleation sites. One type is inert nucleant particles that do not react with the metal matrix during nucleation; however, crystallographic relationships may apply between the particles and matrix. The other type is reactive nucleant particles, like peritectic-based systems. Such particles react with the matrix through chemical reaction or atomic diffusion.

In 1952, Turnbull[34] proposed that a nucleant particle with an appropriate surface can promote the nucleation of a solid grain. This phenomenon was then named heterogeneous nucleation. At the atomic scale, heterogeneous nucleation starts from atom-by-atom stacking on the nucleant particles, with further growth into a solid grain occurring once an energy barrier is overcome. The more nucleant particles present, the more nucleation events that happen. Most heterogeneous nucleation models have been developed based on nucleation over a particle. Some representative models are summarized in Figure 5. According to the classical flat particle model, the minimum values (d) of particle size (or surface area) should reach $2r^*\sin\theta$ (or $\pi(r^*\sin\theta)^2$) (Figure 5(a)), where r^* is the critical nucleus radius and r represents the radius of a growing nucleus. Theoretically, any flat particle, with a d value satisfying $2r^*\sin\theta < d < 2r^*$, can serve as a nucleation site. However, the nuclei that form on these particles possibly fail to grow into solid grains.[34] Such particles and those with d values slightly larger than $2r^*$ are termed "patches" by Turnbull.[34] If d is larger than $2r^*$, any nucleus that forms on the patches with $r > 2r^*\sin\theta$ survives and grows within the undercooled metal melt to form a solid grain. In contrast, if d is smaller than $2r^*$, the nucleus cannot turn into a transformation nucleus even though it grows to the patch boundary, because any further growth along the normal of the surface decreases curvature.[34] Therefore, a critical condition, $d = 2r^*$, is derived for the nucleus to survive and form a grain.[39]

For a given nucleating system, the minimum and maximum undercoolings available in the melt are determinate. The size range of activated nucleant particles can be defined. Using a geometrical factor $f(m, x)$, Fletcher[53] studied the size effect of spherical particles on nucleation rate (Figure 5(b)).

$$f(m,x) = 1 + \left(\frac{1-mx}{g}\right)^3 + x^3\left\{2 - 3\left(\frac{x-m}{g}\right) + \left(\frac{x-m}{g}\right)^3\right\} + 3mx^2\left(\frac{x-m}{g} - 1\right) \quad [2]$$

where $m = \cos\theta$, $x = d/r^*$, and $g = (x^2 - 2mx + 1)^{1/2}$. Similarly, the effect of other particle morphologies, *i.e.*, concave (Figure 5(c), faceted (Figure 5 (e)), and spherical (Figure 5(f)), on nucleation can be discussed using different shape factors. Although various geometrical models for heterogeneous nucleation have been proposed, it must be emphasized that the wetting angle (θ) is essential in all such models. However, these models/criterion developed based on θ are not applicable for small θ (*i.e.*, $\theta \approx 0$ deg).[54] To solve this problem, Chalmers[55] developed an adsorption model (Figure 5(d)), which was then experimentally verified by the nucleation of Al on a monolayer of $TiAl_3$[55] and

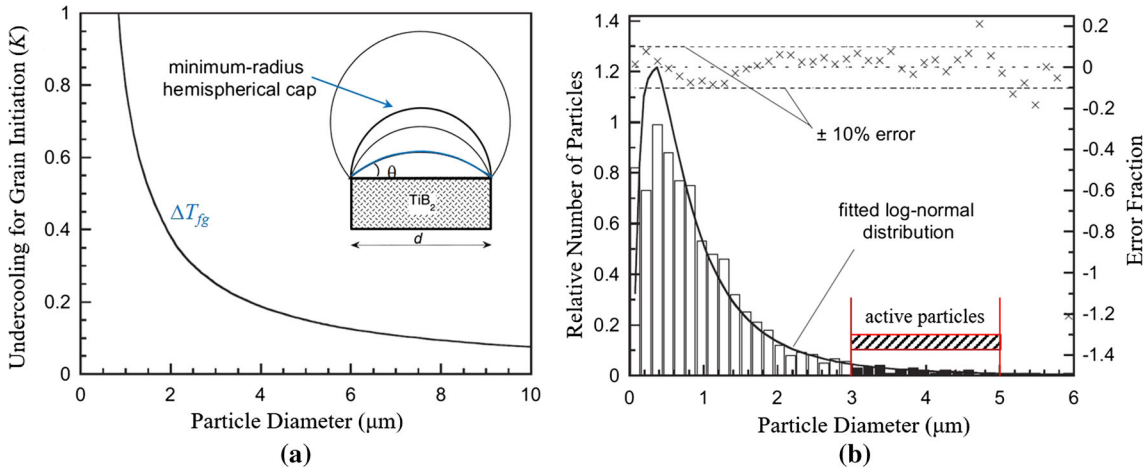

Fig. 4—(*a*) The solid bold curve shows the free-growth undercooling (ΔT_{fg}) available for grain initiation, redrawn from Ref. [1,6]. (*b*) The size distribution of TiB_2 nucleant particles in a commercial Al-5Ti-1B grain refiners.[1] Inset in (**a**) shows a cap-shaped α-Al grain nucleating and growing on a TiB_2 particle with a critical hemispherical dimension.[6] (Reprinted with permission from Ref. [1,6]).

Si on a monolayer of AlP.[56,57] However, Chalmers did not provide an accurate description of the atomic interaction across the nucleating interface between the nucleus (or matrix) and particle. Recently, Fan[58,59] developed an analytical epitaxial model (Figure 5(g)), which shows that (a) a pseudomorphous solid (PS) layer exists between the grain matrix and nucleant particle, and (b) the misfit dislocation decreases the elastic strain energy in the PS layer. From these nucleation models, it can be concluded that the nucleant particles should meet geometrical requirements to enable grain nucleation. Meanwhile, the nucleation barrier must be offset through a favorable atomic configuration at the matrix/particle interface. Misfit dislocation is one such configuration. Furthermore, these nucleant particles contribute to grain refinement by enhancing grain nucleation.

B. *Solute-Restricted Grain Growth*

Three alloy parameters have been widely used to analyze the effects of CS on as-cast microstructures. These parameters are the supercooling parameter (P), growth restriction factor (Q), and freezing range (ΔT). For linear phase diagrams, P, Q, and ΔT values can be calculated using the approach shown in Figure 6.[27] P is the equilibrium freezing range of an alloy,[60] and designated as $P = mc_o(k-1)/k$, where m, c_o, and k represent the liquidus gradient, initial concentration of bulk liquid, and equilibrium partition coefficient, respectively. Meanwhile, $Q = mc_o(k-1)$ was originally derived by Maxwell and Hellawell (equal to 1/X in Reference 37) from the approximation of a diffusion equation for spherical precipitates. Hellawell *et al.*[61,62] correlated Q with the amount of CS available during solidification. Johnsson *et al.*,[18] Lee *et al.*,[24] Bermingham *et al.*,[52] and Liu *et al.*[27] calculated the Q values of major solute elements in liquid Al, Mg, Ti, and Zn, respectively. Their calculations revealed that Ti, Zr, B, and Ag generate large Q values of approximately 33 for Al, 13.6 for Mg, 130 for Ti, and 19.1 K for liquid Zn. However, Easton and StJohn[63] found that it was actually the P value that reasonably characterized the amount of CS. Thereafter, many new theories[2,63–65] were established to explain grain growth, grain size, and CS in grain refinement. These theories are primarily based on the Q value in cast/wrought alloys. Abdel-Reihim *et al.*[66] correlated ΔT with the time delay necessary for the nucleant particles to become effective. The longer the time delay, the more nucleant particles that function as crystallization centers.[66]

Tiller and colleagues[67] derived the solute distribution profile in front of the S/L interface using Eq. [3].

$$C_L = C_o[1 + (1-k)k^{-1}\exp(-vx/D_L)] \qquad [3]$$

where D_L, v, and C_L represent the diffusion coefficient, growth velocity, and distribution of solute concentration ahead of the S/L interface, respectively. When a solid grain grows continuously, a solute build-up zone will form in front of the S/L interface because of solute rejection.[21,68] StJohn *et al.*[2] explained the relationship between CS and solidification pathway along grain growth, as demonstrated in Figures 7(a) through (c). The CS zone develops when the slope of the actual temperature in front of the S/L interface is smaller than that of the equilibrium liquidus temperature.[21] From a mathematic point of view, the CS zone can form if the criterion required to develop a CS zone satisfies the following equation[21,68]:

$$G/V < -mc_o(k-1)/kD \text{ or } GD/V < -mc_o(k-1)/k = P \qquad [4]$$

Otherwise, there is no CS zone formed in the built-up solute field. During the solidification process at a lower cooling rate, the length of the CS zone should be considered, because it affects the growth of both growing grains and subsequently formed grains. For dendritic or cellular growth, Eq. [4] is usually used to evaluate the interfacial instability.[69] As the ratio of temperature gradient to growth velocity (G/V)

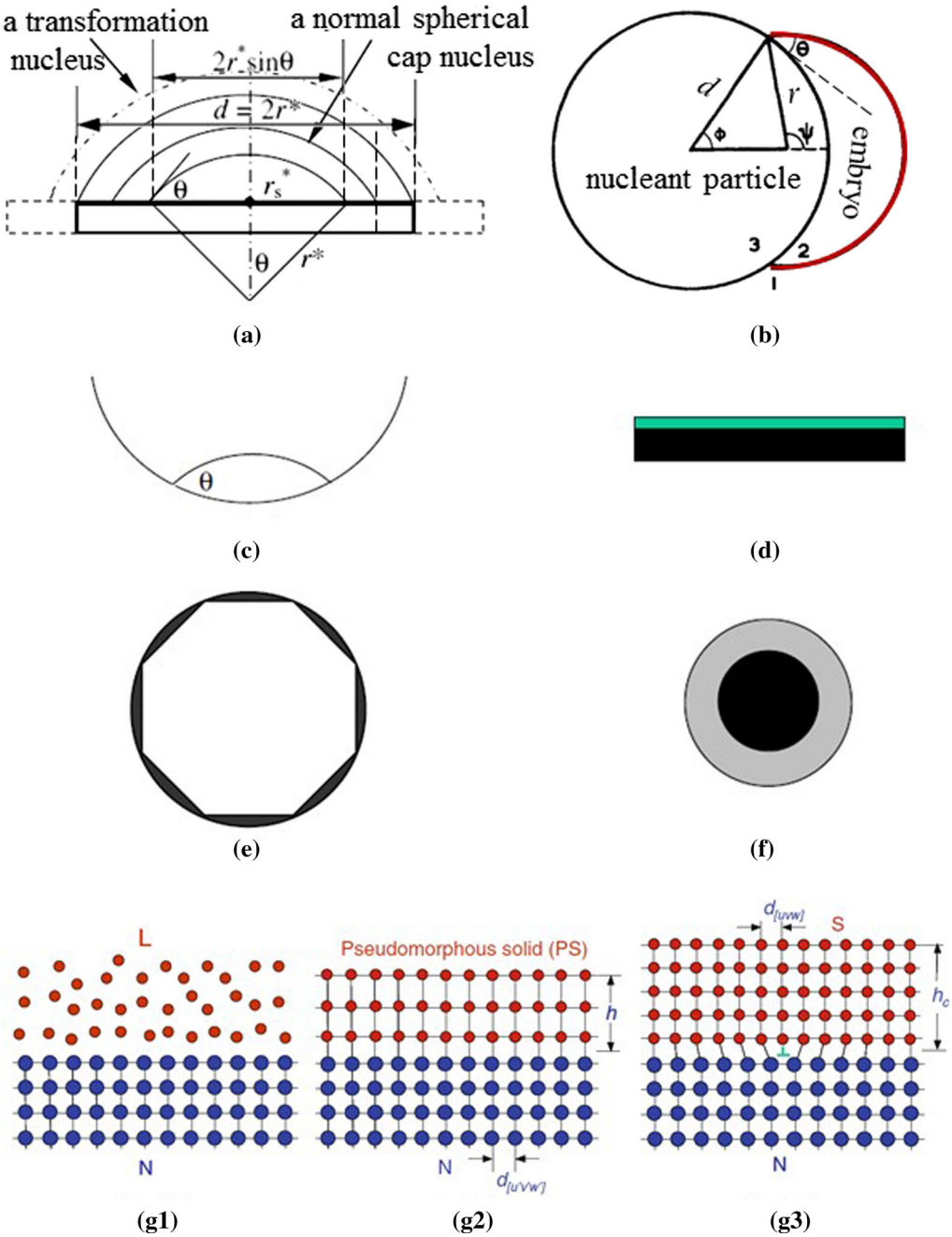

Fig. 5—Schematic illustration of various models proposed for the heterogeneous nucleation on different nucleant particles (or substrates): (*a*) Turnbull's patch model, nucleation initiates on a flat particle;[34] (*b*) Fletcher's convex particle model, embryo 2 nucleates on particle 3 in liquid metal 1;[53] (*c*) the concave particle model, nucleation occurs on a concave particle:[55] (*d*) Sundquist's adsorption model, nucleation starts from an adsorbed layer of atoms on a flat particle;[55] (*e*) Maxwell-Hellawell's model, combining the spherical-cap model and the wetting on a faceted particle:[37] (*f*) the solid-wettable spherical particle model, a uniform layer of condensed liquid film/drop forms on a wettable spherical particle;[47] (*g*1)–(*g*3) Fan's epitaxial model (see details in the text), nucleation begins from an epitaxial growth of a pseudomorphic atomic layer on the potent nucleant particles.[58,59] (Reprinted with permission from Ref. [47,58]).

decreases, the planar interface transitions into cellular, followed by dendritic.[69,70] Most recently, StJohn *et al.*[71] advanced understanding of the role of CS in grain formation. According to their theory, CS facilitates the formation of a nucleation-free zone (NFZ) around each nucleated and growing grain. Interaction of the diffusion fields results in the accumulation of the solute between the growing and newly nucleated grains. Solute accumulation will, in turn, influence the size of the NFZ. Figures 8(a) and (b) show the composition and temperature profiles during solute accumulation. Meanwhile, when temperature fluctuations occur because of convection, the CS zone resists the effects of convection. Any additional nucleation within the CS zone stagnates provided that the amount of CS (ΔT_{cs}) < ΔT_n. This leads to protection of the growing grains from

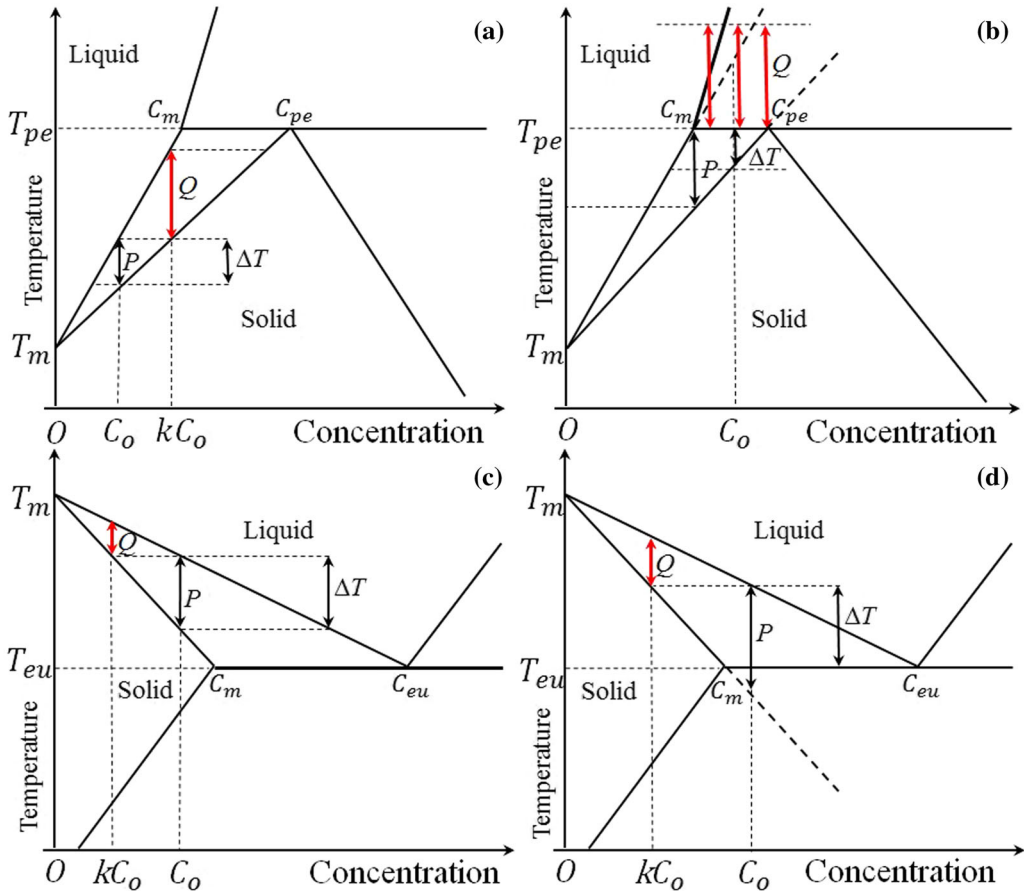

Fig. 6—Illustration of how to calculate the effective P, Q, and ΔT values in peritectic and eutectic systems, respectively, for (*a*) $C_o < C_m$, peritectic system; (*b*) $C_m < C_o < C_{pe}$, peritectic system; (c) $C_o < C_m$, eutectic system; (d) $C_m < <Co < <C_{eu}$, eutectic system. (Reprinted with permission from Ref. [27]).

remelting, allowing them to grow steadily. Higher Q values result in better protection, which contributes to a finer grain size. To obtain a high degree of protection during solidification, it is feasible to manipulate the boundary of the CS zone, alloy chemistry, temperature gradient, and thermal and/or compositional convection.[71] For CS-related solidification in grain refinement, it seems difficult to separate nucleation completely from growth; these processes may actually happen simultaneously in some circumstances. Wang and co-workers investigated the effects of solute on the thermodynamic driving force (ΔG_n) for nucleation in grain refinement of Al alloys.[19] Using CALPHAD-based thermodynamic modeling, they defined ΔG_n and calculated the ΔG_n values of seven binary Al-X alloys (Figures 9(a) and (b)), where X represents four peritectic-forming solute elements, *i.e.*, Ti, V, Nb, and Zr, and three eutectic-forming solute elements, *i.e.*, Cu, Mg, and Si. ΔG_n occupies part of ΔG. At a given small undercooling, increasing solute concentration causes a decrease of ΔG_n. Compared with the eutectic-forming solute elements, addition of peritectic-forming solute elements (particularly Ti) produces a higher initial nucleation rate because of the larger ΔG_n values.[19] Meanwhile, Ti displays the largest Q value among all solute elements in the binary Al-X alloys. Thus, it considerably restricts the grain growth and promotes subsequent nucleation within the CS zone. However, it remains unclear whether such thermodynamic discrepancy between peritectic- and eutectic-forming solute elements exists in other grain refining alloys.

IV. CURRENT THEORIES OF GRAIN REFINEMENT

Over the past six decades, extensive work has been conducted to investigate mechanisms of grain refinement and develop new grain refiners. New scientific knowledge and experimental results have been obtained from grain refinement of Al, Mg, Ti, Fe, Cu, Zn, and their alloys. However, there is still no consensus on the mechanisms of grain refinement. This is mainly attributed to three reasons: (1) grain refinement is affected by both melting and casting conditions; (2) impurities are always difficult to avoid; and (3) unknown physical and chemical interactions exist in metal melts. Regardless of the theories proposed to explain grain refinement, multiple basic questions must be addressed, including: What are the requirements of particles to act as nucleation sites for cast metals? How can the particles be activated as effective nucleation sites? How does the

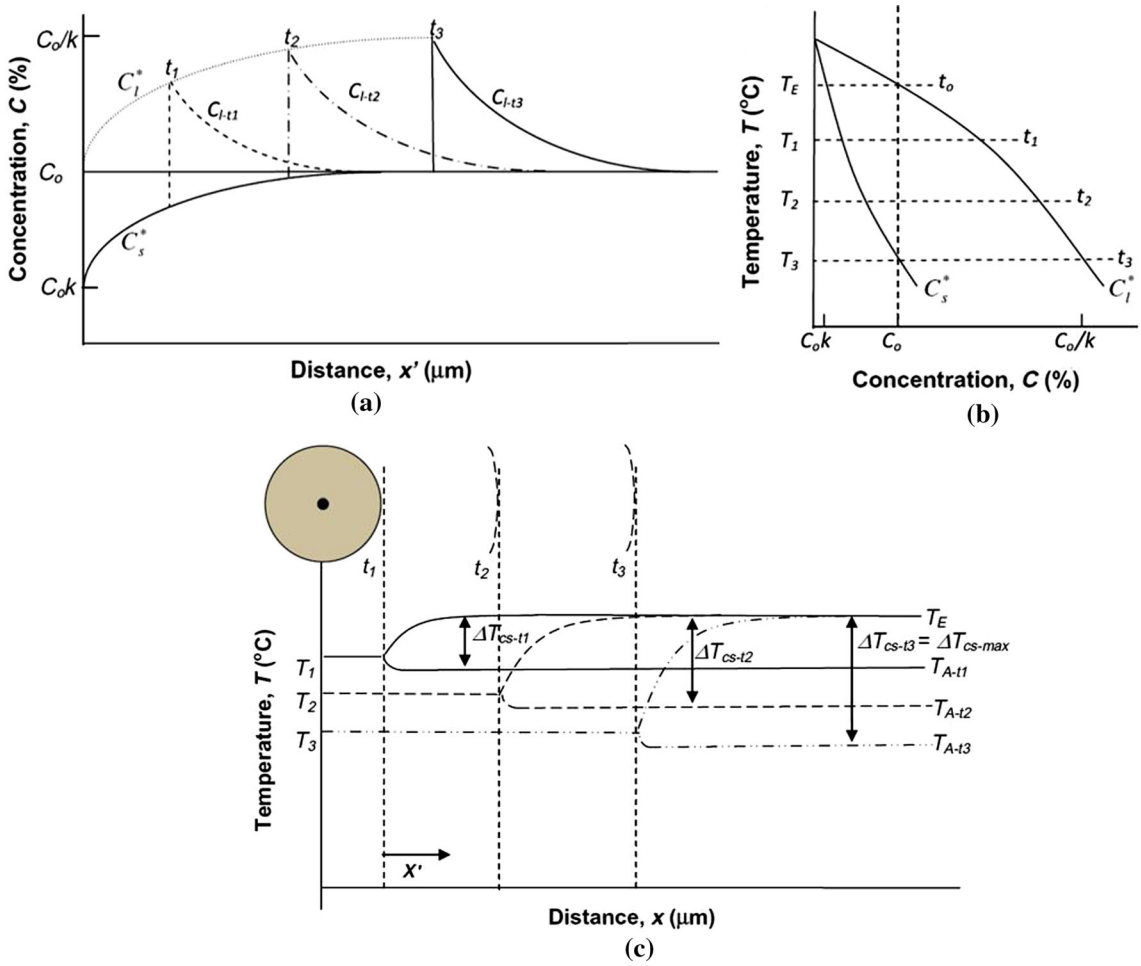

Fig. 7—Schematic illustration of constitutional supercooling (CS) vs. solidification pathway in an alloy with initial composition C_o:[2] (*a*) evolution of solute concentration (C_l*) at the solid/liquid interface from initial state (*t*0) to steady state (*t*3); (*b*) a typical binary phase diagram demonstrating the freezing range from *t*0 to *t*3; (*c*) the evolution of CS-zone from *t*1 to *t*3 at a flat temperature gradient during continuous grain growth. The slight curvature of $T_{A-t1/t2/t3}$ in (**c**) is based on an assumption of equiaxed grain growth, in which the growing grains are a bit hotter than surrounding liquid due to latent heat.[21] (Reprinted with permission from Ref. [2]).

nucleus of cast metals nucleate on the activated particles? Which factors, *i.e.*, solute segregation, convection, and cooling rate, play dominant roles in restricting grain growth? What kind of grain refiners have high efficacy? What is the role of lattice matching between nucleant particles and metal matrix? Many theories have been established to answer these questions. Some typical theories are summarized in Table I. The current theories can be concisely divided into four categories: (1) peritectic-related theories, (2) the hypernucleation theory, (3) inert nucleant theories, and (4) CS-driven theories. These four categories of theories are defined and discussed critically below.

In peritectic-related theories, nucleation initiates on the properitectic particle and further undergoes a peritectic-like reaction. Normally, the properitectic particles form *in situ* prior to peritectic reaction. Peritectic reactions have been widely used to prepare cast metals[23] and functional materials.[72] Based on the solidification of Sb, Ag, and Cu alloys, Asato *et al.* first conceptualized the peritectic reaction theory. Then, this theory was extended to describe grain refinement of Al alloys by Al_3Ti[73] and Al_3Zr/Al_3Nb.[74,75] Similarly, Emley[76] also used peritectics to explain the grain refinement of Mg-Zr alloys. Peritectic reaction is very common in binary alloy systems such as Al-Ti, Cu-Co, Zn-Ag, Fe-Ni, and Mg-Zr alloys. As a result, the peritectic reaction theory and its application to grain refinement possess much scientific and technological importance, although its roles in grain refinement are still under debate.[77] Both the peritectic hulk theory[78,79] and duplex nucleation theory[56,80] differ somewhat from the peritectic reaction theory; however, the essence of these two theories is also based on peritectic reaction. Theoretical discrepancies between the peritectic reaction, peritectic hulk, and duplex nucleation theories and their associated applications are listed in Table I.

The hypernucleation theory was firstly proposed by Jones and Pearson[81] while investigating grain refinement of α-Al. After calculating the individual activities of Ti in Al melts and TiB_2 particles, Jones and Pearson speculated that the segregating Ti atoms at the TiB_2/melt interface formed a layer of Al-Ti pseudo-crystals

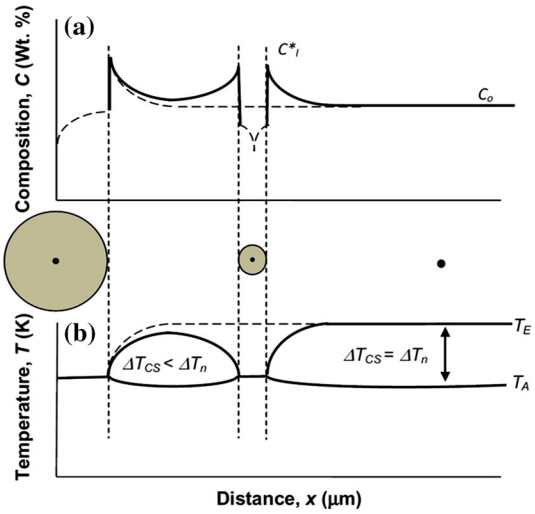

Fig. 8—Schematic graphs showing (*a*) the composition profile and (*b*) the CS zone boundary between, and in front of, the newly nucleated grains, which are resulted from solute accumulation. Additional nucleation between these grains is not feasible while $\Delta T_{cs} < \Delta T_n$. (Reprinted with permission from Ref. [71]).

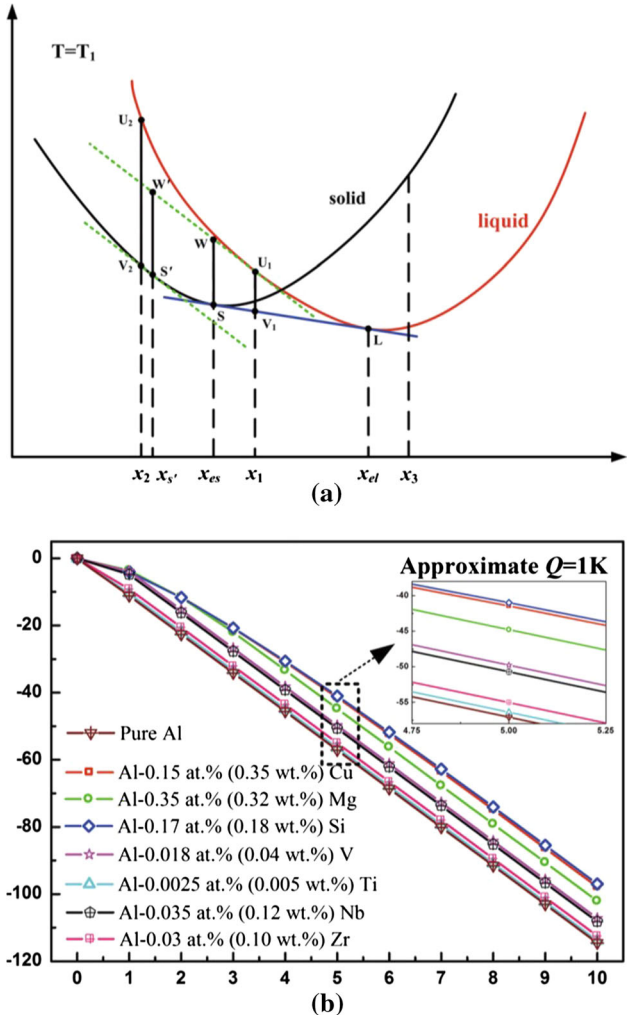

Fig. 9—(*a*) Definition of the thermodynamic driving force (ΔG_n) for nucleation of solid grain from liquid metal; (*b*) Calculated ΔG_n values of seven peritectic- or eutectic-forming solute elements in the Al alloy systems at a given small Q value (~1K), plotted against undercoolings.[19] ΔG_n values of solid grains with concentrations x_{es} and x_s, nucleating from liquid metal with concentrations x_1, are WS and W'S', respectively. U_1V_1 (or U_2V_2) represents the Gibbs free energy change per mole (ΔG) at concentration x_1 (or x_2) at equilibrium state.[19] (Reprinted with permission from Ref. [19]).

on TiB_2. Such pseudo-crystals help to release the elastic strain energy through misfit dislocations. Thus, α-Al grains are able to nucleate on these pseudo-crystals at very small undercooling. Similarly, Fan[58,59] developed an epitaxial nucleation theory, in which nucleation begins from epitaxial growth of a pseudomorphic atomic layer on a particle. Details of Fan's epitaxial nucleation theory and associated experimental validation have already been given in Section III–A. This epitaxial nucleation theory is similar to the hypernucleation theory.

In the inert nucleant theories, nucleation starts on an inert particle through heterogeneous nucleation. Different from the properitectic particle, there is no reaction between the inert nucleant particle and matrix grain during nucleation, although both involve heterogeneous nucleation. In other words, inert nucleant particles and properitectic particles serve as inert and reactive nucleation sites, respectively. Regarding the inert nucleant theories of grain refinement, the boride/carbide and lattice matching theories are the two most common. In the boride/carbide theory,[4,13] grain refiners are directly added to a metal melt to achieve grain refinement. These grain refiners were selected without much crystallographic consideration, but with a preference for thermodynamic stability[82,83] For instance, Mg-Al alloy was refined using C_2Cl_6 and C_6Cl_6[76] and AZ31 and AZ61 alloys were refined by Al_4C_3 and SiC.[84] The lattice matching theory, *i.e.*, the E2EM matching model, is a more convenient approach to predict new grain refiners from first principles than the boride/carbide theory. The lattice matching theory hypothesizes that the nucleation in grain refinement can be promoted through good crystallographic matching, because good lattice matching lowers the nucleation barrier.[35] Regarding its application, the lattice matching theory has been experimentally validated for Mg-Al alloys, which can be refined by Al_2Y,[85] AlN,[86] and Al/Fe-enriched particles.[87] Additionally, Mg-14Li-1Al alloys were refined by TiB_2 and Al_3Ti.[88] In these experimental systems, good lattice matching exhibited between the alloy matrix and nucleant particles. Despite this, not all types of particles that match well with their counterpart metal matrix definitely display efficient grain refinement.

The CS-driven theories explain grain refinement based on the hypothesis of CS-driven nucleation on effective particles.[13,63] These theories have experienced two periods of development: the solute paradigm and the interdependence theory. The solute paradigm theory elaborates the effect of solute on grain refinement from two perspectives: (1) the growth of grains can be restricted by the segregating solute at their S/L

Table I. The Current Representative Theories on the Grain Refinement of Cast Metals

Theory		Mechanism	Application
Peritectic-related theories	peritectic reaction	α-Al nucleates on Al_3Ti through peritectic reaction $Al(l) + Al_3Ti \rightarrow$ α-Al(s)[73,80]	Al alloys refined by Al-Ti master alloy[73]
		Mg nucleates on Zr particle *via* peritectic reaction Mg(l) + α-Zr→α-Mg(s)[76]	Al/Mn/Si-free Mg alloys refined by Zr[76]
	peritectic hulk	boride shell retards the dissolution of Al_3Ti to promote nucleation of α-Al by peritectic reaction[78]	partially verified by experiment, opposite to Mayes *et al.*' result[79]
	duplex nucleation	a thin layer of Al_3Ti over TiB_2 act as nucleation site for α-Al undergoing peritectic reaction[80]	convinced by Schumacher *et al.*[56]
Hyper-nucleation theory		segregating Ti atoms at TiB_2/melt interface enhances the nucleation of α-Al on pseudo-crystals[81]	similar to Fan's epitaxial model and experimental results[58,59]
Inert nucleant theories	boride/carbide theory	α-Al nucleates on AlB_2, TiB_2, and (Al,Ti)B[4,13]	pure Al refined by Al-Ti-C and Al-Ti-B master alloys
		Mg nucleates on either Al_4C_3 or other compounds containing Al, C, andO[82,83]	1. Mg-Al alloy refined by C_2Cl_6 and C_6Cl_6,[76] 2. AZ31 and AZ61 alloy refined by Al-Al_4C_3-SiC[84]
	lattice matching	nucleation can be enhanced by the good lattice matching between nucleant particle and metal matrix[35]	1. Mg-Al alloys refined by Al_2Y,[85] 3. Mg-Al alloys refined by AlN,[86] 4. Mg-Al alloys refined by Al/ Fe-rich particles,[87] 2. Mg-14Li-1Al alloy refined by TiB_2 and Al_3Ti[88]
CS-driven theories*	solute paradigm	both potent nucleants and segregating solutes are essential to generate grain refinement[13,63]	1. Al alloys refined by Al-Ti-B master alloy,[13] 2. Mg-Al(-Mn) alloys refined by SiC and Al,[83] 3. Grain refinement of steel by Jackson[51], 4. Titanium alloys refined by native particles and Si/B/Be solutes[52,90,91]
	interdependence theory	gain size depends on (a) a nucleation-free zone and (b) an interparticle spacing[2]	validated in the Al and Mg alloys refined by TiB_2[2]

*CS represents constitutional supercooling. Compared with the solute paradigm, the interdependence theory developed a rigorous physical background, linking grain formation and nucleant selection together.

interfaces, and (2) the CS generated by growing grains induces new nucleations on other nucleant particles once a critical ΔT_n is reached.[13,36,89] These potent nucleant particles pre-exist in the CS zone. However, Men and Fan[65] concluded that new nucleations only appear on the particles outside the CS zone (part of diffusion zone). In 1972, Jakson [51] had already realized that both solute and particles are essential in the grain refinement of steels. However, he did not describe how the solute accumulation affects grain nucleation and/or growth. In 1993, Johnsson[18] first proposed the solute paradigm in Al alloys. This paradigm was further developed by Easton and StJohn using an empirical Q-value model.[63] The Q value was defined in Section III–B. According to the solute paradigm theory, the as-cast grain size can be semi-quantified as a linear function of $1/Q$. Even as a phenomenological theory, validation and application of the solute paradigm were convincing in some experimental reports, such as Mg-Al(-Mn) alloys refined by SiC,[83] Al alloys refined by Al-Ti-B master alloy,[13] Ti alloys refined by Si/B/Be,[52,90,91] and Mg refined by Zr.[24] Along the lines of the solute paradigm, StJohn *et al.*[2] developed an interdependence theory to reveal the physical background between grain formation and nucleant selection. This is a recent breakthrough in grain refinement. The interdependence theory assumes that grain formation results from the interdependence effect between nucleation and growth, which act in concert within an alloy chemistry environment. The final grain size mainly depends on (a) a NFZ where nucleation stagnates, and (b) an additional distance to the nearest most effective particle.[2] Mathematical expression of these two components will be addressed in Section V. Through controlling alloy chemistry and/or growth rate, the NFZ can be minimized so as to promote grain refinement.[2,71] All the theories in Table I have been

successfully used to explain some experimental results and observed phenomena. However, it is still difficult to use any single theory to explain all experimental results. Moreover, some new grain refiners developed based on these theories do not always produce efficient refining results. Thus, there must still be some other unknown factors that also contribute to grain refinement.

V. MODELING OF GRAIN REFINEMENT FOR CAST METALS

Grain refinement in cast metals is subject to many complex factors like nucleation, particle size, size distribution, particle morphology, solute and thermal fields, undercooling, holding time, casting temperature, convection, and capillarity effects. A number of models have been developed to describe/predict the microstructural evolution in grain refinement. Generally, modeling of grain refinement at the microscopic scale can be classified into two categories: *i.e.*, deterministic and probabilistic approaches. This paper only reviews modeling of the inoculation-induced grain refinement of cast metals; other issues like the solid-state process and external fields are not considered. The major assumptions used in deterministic and probabilistic modeling are listed in Table II. The deterministic approach proposes that the number of grains nucleating in the bulk metal liquid is a function of undercooling.[2,6,37,39,51,92–94] Expression of this function is deduced from experimental parameters; *i.e.*, the cooling curve and grain density. The probabilistic approach is based on interfacial energy minimization, where complex variations (such as the size distribution of nucleant particles and the impingement of adjacent grains) are treated as a random function.[100,102–104,106] However, such functions do not include the anisotropy of interfacial energy. To obtain accurate description/prediction, both deterministic and probabilistic models are often combined in applications.

A. *Deterministic Modeling*

Some predictive models to interpret the deterministic nature of grain formation have been formulated. Maxwell and Hellawell originally developed a simple model (denoted the M-H model) to explain the grain refinement in the binary peritectic alloy systems Al-Ti, Al-Zr, and Al-Cr.[37] The M-H model incorporates and quantifies the ability of specific parameters to decrease grain size. These parameters consist of alloy constitution, substrate activity, wetting angle, cooling rate, and latent heat. Some characteristic parameters of the M-H model are shown in Figure 10. At the initial stage of nucleation in an isothermal melt before recalescence, the nucleation rate increases as temperature lowers (see Figure 10(a)). Before the nucleation rate drops obviously, it is assumed in this model that the grains in a recalescent melt grow with a spherical shape.[37] Such spherical growth is actually treated in an immediate and continuous diffusion-controlled manner. After recalescence starts, the nucleation rate will lower due to the decrease of undercooling. Meanwhile, recalescence also suppresses activation of the nucleant particles available in a system. Using an invariant size approximation, the radius of a spherical grain (R) is given by Eq. [5],

$$R = \lambda_s (D_s t)^{1/2} \qquad [5]$$

In Eq. [5], $\lambda_s = f(S)$ and $S = 2(C_{IL} - C_A) / (C_{IS} - C_{IL})$, where S, D_s, t, C_A, C_{IL}, and C_{IS} are the growth parameter, the diffusion coefficient of solute in the liquid, the growth time, the solute concentration of bulk liquid, the solute concentration of liquid at the S/L interface, and the solute concentration of solid at the S/L interface, respectively.[37] These parameters are schematically illustrated in Figure 10(b). In peritectic alloy systems, the growth of spherical grains obeys a function of melt undercooling (ΔT) below the temperature for peritectic reaction ($T_{peritectic}$). If k defines the equilibrium distribution coefficient (constant) and $m = (T_{eq} - T_{Al}) / C_A$, then $C_{IL} = C_A - \Delta T/m$ and $C_{IS} = kC_{IL}$. ΔT is the undercooling relative to $T_{peritectic}$. When considering growth at small undercooling, the thermal undercooling (ΔT_t) and kinetic undercooling (ΔT_k) are neglected in the M-H model. However, the CS (ΔT_{cs}) and curvature undercooling (ΔT_r) have to be taken into account because of their obvious influence on grain refinement. Normally, ΔT_{cs} arises from solute accumulation in front of an advancing S/L interface. For instance, ΔT_{cs} is ~$2.5 \times 10^{-5}/R^{-1}$ in Al. Thus, the equilibrium temperature of a spherical grain with a radius of 1 μm will be depressed by ~0.25 deg.[37] At

Table II. The representative Deterministic- and Probabilistic Models and Their Respective Fundamental Assumptions

Model	Category	Micro-segregation	Growth kinetics	*CS*	*TS*
Maxwell-Hellawell[37]	deterministic	no	diffusion-limited spherical growth	no	yes
Easton-StJohn[51,63]	deterministic	yes	CS-driven		
Qian *et al.*[96]	deterministic	yes	spherical growth + planar growth	yes	no
Greer *et al.*[6,39]	deterministic	yes	spherical growth	yes	no
StJohn *et al.*[2]	deterministic	yes	CS-driven + NFZ	yes	no
Martorano-Biscuola[100]	probabilistic	no	instantaneous nucleation	no	yes
Rappaz-Gandin[104]	probabilistic	no	dendrite tip	restricted	no
Wang *et al.*[106]	probabilistic	yes	dendrite fragmentation	yes	yes
Yao *et al.*[102]	probabilistic	yes	CS-driven	yes	no

CS, TS, and NFZ are designated to be constitutional supercooling, thermal supercooling, and nucleation freezing zone, respectively.

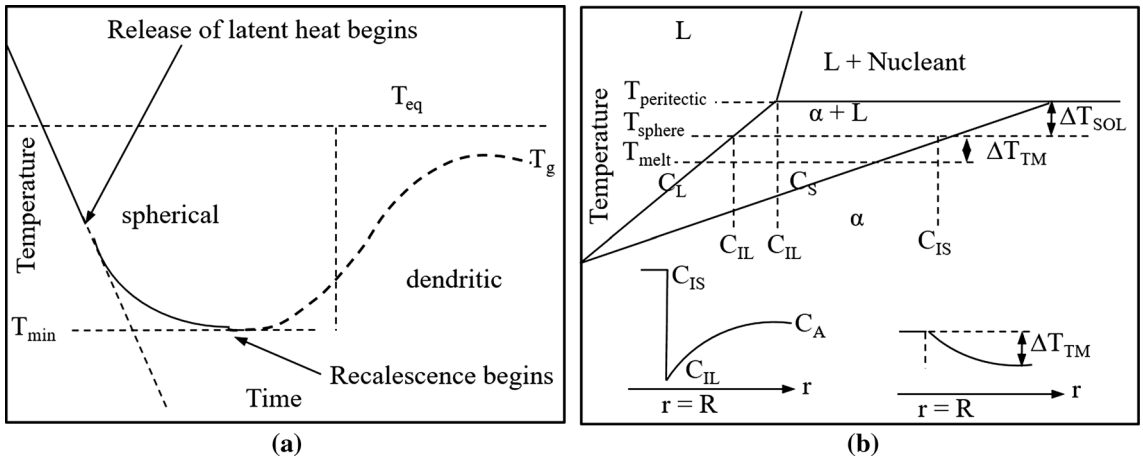

Fig. 10—Schematic illustration showing (*a*) the formation of cooling curve and (*b*) the parametric definition of the M-H model. (Reprinted with permission from Ref. [37]).

such undercooling, the nucleation rates will change appreciably. While ignoring ΔT_t and ΔT_{cs}, S can be rewritten. The term S defined by Maxwell and Hellawell to describe grain growth during peritectic solidification was further derived as

$$S = \frac{-2(\Delta T - \Delta T_r)/m}{(k-1)[C_A - (\Delta T - \Delta T_r)/m]} \quad [6]$$

where m is the liquidus slope and ΔT_r represents curvature undercooling. ΔT_r should not be neglected when small grains nucleate and grow at small undercooling. Using the M-H model, Maxwell and Hellawell further investigated the individual contributions of particle activity, cooling rate, alloy system, and nucleant size. The M-H model indicates that at a given small cooling rate, the efficiency of a grain refiner mainly depends on wetting angle and CS. Beyond a critical ratio of grains to nucleant particles, further addition of grain refiner only leads to marginal grain refinement.[37] More quantitative experimental data are required to validate the M-H model, although it has some value in predicting the grain refinement of cast alloys.

CS is also named constitutional undercooling in some circumstances. Chalmers[92] proposed a CS-driven nucleation model based on the assumption that CS helps to trigger nucleation on the nucleant particles available in metal melts. At a negligible temperature gradient, the CS-driven nucleation mechanism has been recognized as a dominant mechanism in the presence of a grain refiner. Based on the CS-driven nucleation mechanism, Easton and StJohn[63] derived an equation (termed the E-S model) to calculate the relative grain size (RGS). RGS is also defined as the solid fraction (f_{sn}) at which the amount of CS (ΔT_{cs}) reaches the critical undercooling required for nucleation (ΔT_n).

$$\mathrm{RGS} = f_{sn} = 1 - \left(1 - \frac{\Delta T_n}{m \cdot c_o}\right)^{1/(k-1)} \quad [7]$$

$$f_{sn} = \Delta T_n / Q \quad [8]$$

in which c_o represents the overall solute concentration, and $Q = mc_o(k-1)$ is the growth restriction factor (see Section III–B).[63] To some extent, this early E-S model reflects the contribution of solute additions to the resulting RGS. Coincidently, various experimental data identified a nearly linear relationship between the as-cast average grain size (d_{gs}) and $1/Q$ in binary Al alloys.[18,93] However, f_{sn} and d_{gs} are not exactly equivalent, although they agree with each other from a fundamental perspective. Considering the combined contributions from solute segregation and nucleant particles, Easton and StJohn[94] then developed a semi-empirical modified equation to relate d_{gs} and $1/Q$.

$$d_{gs} = \frac{1}{\sqrt[3]{N_v}} + \frac{b' \cdot \Delta T_n}{Q} \quad [9]$$

In Eq. [9], N_v and b' are the volume density of nucleant particles and a fitting coefficient, respectively. Eq. [9] can be applied on the conditions that (a) grains nucleate at small undercooling, (b) the amount of grain growth must become sufficient to initiate nucleation on other effective nucleants, and (c) the curvature undercooling is ignored. Easton *et al.* [63] concluded that the intercept of Eq. [9] and b' are related to the potency of grain refiners and number of active nucleant particles, respectively. Eq. [9] has been validated for Al castings inoculated with Al-Ti-B master alloys. The early E-S model has two limitations: (1) the kinetic factors that affect solidification are not incorporated, and (2) an actual measured fitting coefficient is required. Despite these limitations, it still is a practical analytical model that provides reasonable explanations for grain refinement in some cast Al alloys,[94] Ti alloys,[52] Mg alloys,[95] and Zn alloys.[27]

Further, Qian *et al.*[96] proposed a model to describe the CS-driven nucleation and formation on a number of nucleant particles in an actual 3-D metal melt. This model has a rigorous physical basis, as shown in Figure 11(a) and (b). Figure 11(a) illustrates the nucleation of a grain on a nucleant

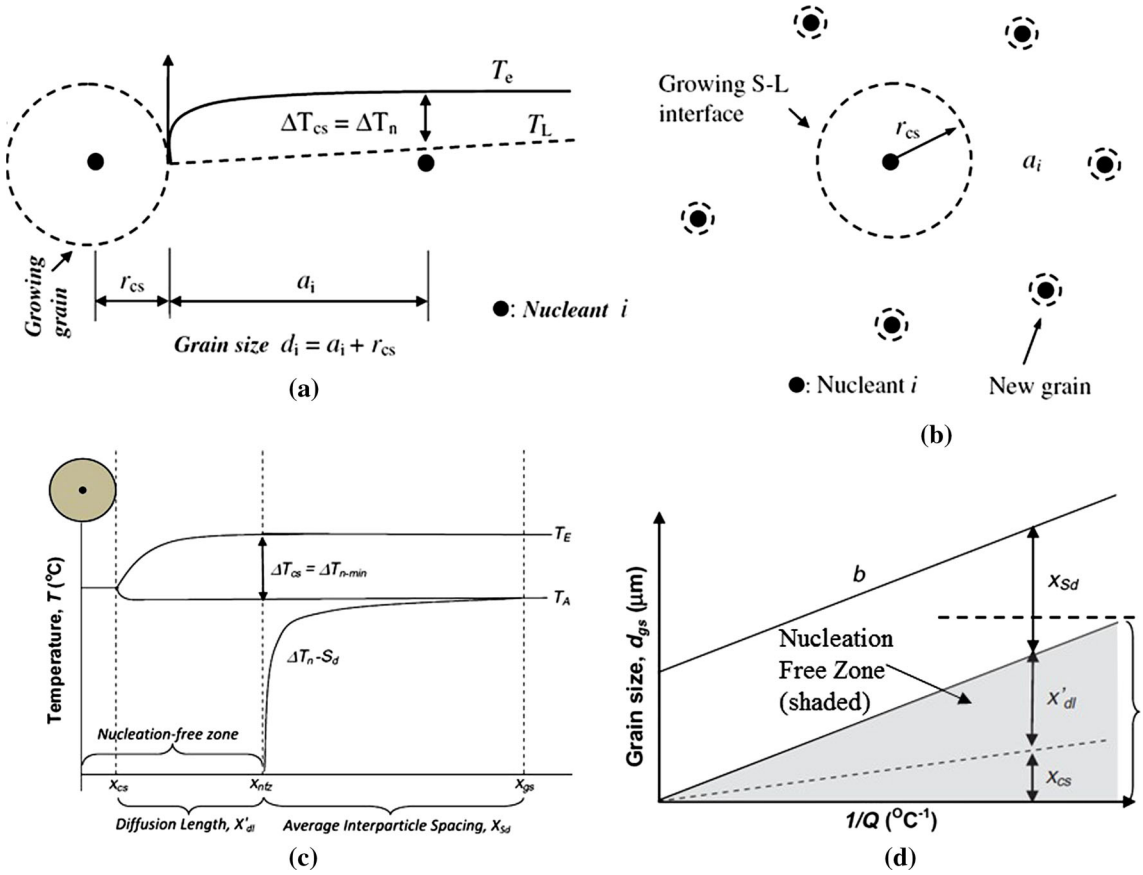

Fig. 11—(*a*, *b*) An illustration of the CS-driven nucleation on single and substantial potent nucleants respectively, with reprint permission from Ref. [96]; (*c*, *d*) Two key components (*i.e.*, nucleation-free zone and interparticle spacing) used in the interdependence theory to predict grain size, with reprint permission from Ref. [2].

particle in the CS zone. During its progressive growth, it induces a CS zone ahead of the advancing S/L interface. Once the grain grows over a critical length r_{cs} ($r_{cs} = D{\cdot}\Delta T_n/(v{\cdot}Q)$) to meet $\Delta T_{cs} \geq \Delta T_n$, the next nucleation occurs on another nucleant i located at distance a_i from the S/L interface. In an actual 3-D metal melt, a number of effective nucleant particles are located around a growing grain, leading to a wave of new nucleations. A cross-sectional view of such 3-D nucleation events in the radial directions is depicted in Figure 11(b). d_{gs} value of the grains involved is written as

$$d_{gs} = \frac{1}{N}\sum_{i=1}^{N} a_i + D \cdot \Delta T_n/(v \cdot Q) \qquad [10]$$

in which N is the total number of nucleating grains surrounding growing grains; D is the solute diffusion coefficient; ΔT_n is the critical undercooling for nucleation; v is growth velocity, and a_i is the distance from the advancing S/L interface.[96] For growing S/L interfaces with curvatures from small to infinite, Eq. [10] has been theoretically verified to be applicable to both spherical and planar growth.[96] Qian *et al.*'s model established a fundamental basis for CS-driven grain formation. Moreover, from a theoretical aspect, it again confirms that d_{gs} varies linearly with $1/Q$.

Recently, StJohn *et al.*[2] made substantial progress in the development of deterministic modeling. Their new model, termed the interdependence theory, was also proposed along the line of CS-driven nucleation.[2] The influence of thermal undercooling had not previously been considered because of the very small cooling rate (~1 K/s[2]). According to interdependence theory, d_{gs} mainly incorporates three factors: the critical radius (x_{cs}) that a grain must reach to achieve ΔT_n for subsequent nucleations, the length of the diffusion field (x'_{dl}), and the average interparticle spacing (x_{sd}). As a simplified version of the interdependence theory, Figure 11(c) clearly demonstrates these three factors that together define d_{gs}.

$$d_{gs} = x'_{dl} + x_{cs} + r_{sd} \qquad [11]$$

in which $x'_{dl} = \frac{D{\cdot}z{\cdot}\Delta T_n}{vQ}$, $x_{cs} = \frac{4.6{\cdot}D}{v}\cdot\frac{C_l^*-C_o}{C_l^*{\cdot}(1-k)}$, and $r_{sd} = \frac{4.6{\cdot}D}{v}\cdot\frac{C_l^*-C_o}{C_l^*{\cdot}(1-k)}$. Eq. [11] can thus be rewritten as

$$d_{gs} = \frac{D \cdot z \cdot \Delta T_n}{vQ} + \frac{4.6 \cdot D}{v}\cdot\frac{C_l^* - C_o}{C_l^* \cdot (1-k)} + r_{sd} \qquad [12]$$

StJohn *et al.*'s model established a mathematical description to relate grain formation and nucleant selection in grain refinement. The first two terms in Eq. [11] and [12] constitute a NFZ, as shown by the

shaded area in Figure 11(d). The NFZ determines the minimum d_{gs} available in a grain-refining system at an infinite particle density (*i.e.*, $x_{cs} \approx 0$).[2] In accordance with its experimental validation, the interdependence theory clearly elucidates mechanisms of grain refinement. Meanwhile, the interdependence theory also reveals directions for future research to develop other efficient grain refiners. It should be mentioned that factors such as geometry and crystallography are not considered in these CS-driven models. However, they uncovered a semi-quantitative relationship between grain formation and nucleant selection for the first time. Other deterministic modeling approaches have also been proposed.[64,65,97] Men and Fan[65] found that in Al-Zn and Al-Si alloys, d_{gs} linearly varies with $(1/Q)^{1/3}$. Most deterministic models, such as those recently developed by Maxwell *et al.*,[37] Easton *et al.*,[63,94] Greer *et al.*,[6,39] Qian *et al.*,[96] and StJohn *et al.*,[2] confirmed the conventional linear relationship between d_{gs} and $1/Q$. These models were also experimentally validated for cast Al,[23] Mg,[24] Ti,[25,52,90,91] Cu,[26] and Zn alloys.[27,98,99] An approach that decreases NFZ will facilitate grain refinement.

B. *Probabilistic Modeling*

In the probabilistic models, the nucleation undercoolings required for equiaxed grains follow either a normal or a log-normal distribution, and have been successfully applied by Martorano and Biscuola,[100] Nastac *et al.*,[101] and Yao *et al.*[102] Martorano and Biscuola proposed a probabilistic model (denoted the M-B model) to predict the columnar-to-equiaxed transition during steady-state solidification. Actually, the M-B model is an extension of the classical model developed by Hunt.[103] In the M-B model, five basic assumptions are made, including (1) linear temperature gradient, (2) spherical growth, (3) potent nucleant particles, (4) instantaneous nucleation, and (5) Gaussian distribution of undercoolings.[100] As shown in Figure 12(a), the velocity (V) of isotherms depends on the growing columnar front, leading to different undercoolings ahead the columnar front. Then, equiaxed grains nucleate and grow to a radius R_g at a radial velocity V_g. Profiles of the volume fraction of equiaxed grains (ε_g) and temperature are illustrated in Figure 12(b), showing the distributions of liquidus temperature (T), nucleation temperatures (T_N), and undercoolings (ΔT_N) on different nucleant particles (i and $i + 1$), and the columnar front undercooling (ΔT_{col}). Considering an equiaxed grain at a given location, it requires an undercooling of ΔT_N when nucleating at time t_N. When $t > t_N$, ΔT at this location is greater than ΔT_N and R_g is then expressed as[103]

$$R_g(\Delta T_N, \Delta T) = \int_{t_g}^{t} V_g dt = \int_{\Delta T_N}^{\Delta T} \frac{A\Delta T^m}{VG} d\Delta T = \frac{A}{VG(m+1)}\left(\Delta T^{m+1} - \Delta T_N^{m+1}\right) \quad [13]$$

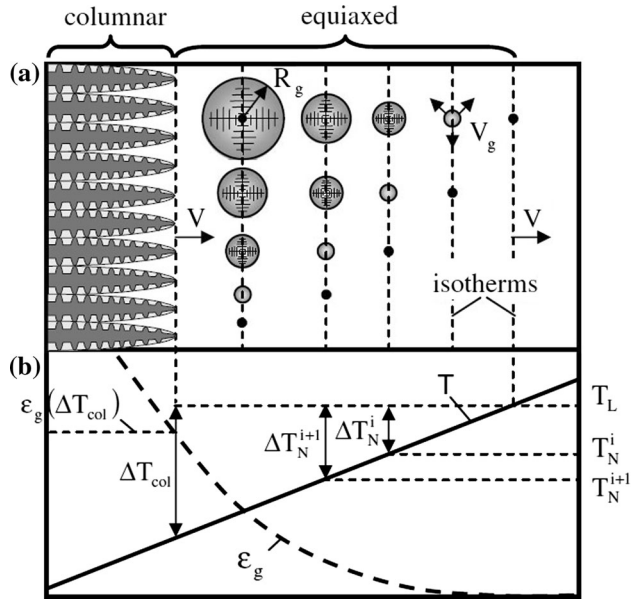

Fig. 12—(*a*) Columnar grains grow at a velocity of V, and equiaxed grains nucleate at a velocity of V_g within the thermal undercooling boundary layer;[100] (*b*) the volume fraction (ε_g) of equiaxed grains and the temperature (T), showing the influence of liquidus temperature, nucleation temperature and undercooling on various nucleant particles.[100] (Reprinted with permission from Ref. [100]).

When ignoring the impingement of equiaxed grains, at the local undercooling (ΔT), the volume fraction of the equiaxed grains that nucleate between ΔT_N and $\Delta T_N + d\Delta T_N$ is given by Eq. [14].

$$d\varepsilon_{gE} = \frac{4}{3}\pi R_g^3(\Delta T_N, \Delta T) dn = \frac{4}{3}\pi R_g^3(\Delta T_N, \Delta T) \frac{dn}{d\Delta T_N} d\Delta T_N \quad [14]$$

Provided that all equiaxed grains nucleating within an undercooling range of $0 \le \Delta T_N \le \Delta T$ are accounted for, then the extended volume fraction (ε_{gE}) of equiaxed grains is calculated as follows[100]:

$$\varepsilon_{gE}(\Delta T) = \int_0^{\Delta T} \frac{4}{3}\pi R_g^3(\Delta T_N, \Delta T) \frac{dn}{d\Delta T_N} d\Delta T_N \quad [15]$$

Using the Avrami correction, the total volume fraction of equiaxed grains at ΔT can be quantified as follows:

$$\varepsilon_g(\Delta T) = 1 - \exp(-\varepsilon_{gE}(\Delta T)) \quad [16]$$

Furthermore, the growth maps for columnar and equiaxed grains can be constructed. The M-B model implies that the distribution of nucleation undercoolings in a unidirectional steady-state solidification system strongly affects the fields of columnar and equiaxed growth.[100]

According to the Gaussian distribution, the undercoolings needed to activate heterogeneous nucleations on potent particles are mathematically expressed as follows[60]:

$$\frac{dn}{d(\Delta T_N)} = \frac{n_T}{\sqrt{2\pi}\cdot\Delta T_\sigma}\exp\left[-\frac{1}{2}\left(\frac{\Delta T_N - \overline{\Delta T_N}}{\Delta T_\sigma}\right)^2\right] \quad [17]$$

where n, n_T, ΔT_σ, and ΔT_N denote the number of active nucleant particles, the total number of nucleant particles available in a system, the standard deviation of undercooling, and the average undercooling to generate nucleation, respectively. During columnar and equiaxed grain growth, the boundary curve in growth maps (see Figure 12) is interpreted using Eq. [18]

$$\varphi = \frac{1}{3(m+1)}\left\{\frac{0.66}{\ln(1-\varepsilon^{\mathrm{block}})^{-1}}\cdot\frac{1}{\Delta T_\sigma/\overline{\Delta T_\mathrm{N}}\sqrt{2\pi}}\int_0^{V^{1/m}}\left[\left[1-\left(\frac{\Delta T_\mathrm{N}}{V^{1/m}}\right)^{m+1}\right]^3\exp\left[-\frac{1}{2}\left(\frac{\Delta T_\mathrm{N}-1}{\Delta T_\sigma/\overline{\Delta T_\mathrm{N}}}\right)^2\right]\right]d\Delta T_\mathrm{N}\right\}^{1/3} \quad [18]$$

where the volume fraction of equiaxed grains ($\varepsilon^{\mathrm{block}}$) is arbitrarily selected as 0.49; V is the relative growth velocity of the columnar front, and the constant m depends on the specific alloy system. Computer simulation using the M-B model shows that increasing the distribution of nucleation undercooling will not facilitate equiaxed growth if both V and ΔT_{col} are greater than unity. However, the equiaxed growth can be enhanced when both V and ΔT_{col} are smaller than unity. Such behavior was confirmed by a stochastic model, which indicated that widening the distribution of nucleation undercooling could transform the columnar grain structures by 50 pct.[100] When assuming instantaneous nucleation conditions, predictions of the columnar-to-equiaxed transitions should be evaluated carefully.

Using a 2-D cellular automata approach,[104] Rappaz and Gandin proposed a model (denoted the R-G model) to reveal the evolution of grain structure during solidification. The R-G model is based on the following assumptions: (a) the nucleant particles at the mold wall and in the bulk liquid are dispersed according to two different distribution functions, (b) the dendrite tip growth, preferential crystallographic orientation, and mechanical impingement of adjacent grains are considered, (c) the temperature gradient in the bulk liquid is uniformly distributed, (d) for the isothermal solidification process, CS (ΔT_{cs}) dominates rather than ΔT_t, ΔT_k, or ΔT_r.[100]

$$\omega = \frac{c^* - c_\mathrm{o}}{c^*(1-k)} = Iv\left(\frac{Rv}{2D}\right) \quad [19]$$

$$R = 2\pi\sqrt{\frac{F}{mG_c\delta_c - G}} \quad [20]$$

where ω is the supersaturation coefficient; c^* is the solute concentration at the dendrite tip; c_o is the overall solute concentration in the liquid metal; R is the dendrite tip radius; D is the diffusion coefficient; δ_c is a parameter close to unity; G_c is solute gradient, and G is thermal gradient. G can be ignored during equilibrium solidification.[105] The relationship between undercooling and supersaturation can be expressed by Eqs. [21] and [22]

$$\Delta T = mc_\mathrm{o}\left[1 - \frac{1}{1-\omega(1-k)}\right] \quad [21]$$

$$L(t) = \int_{t_N}^{t} v[\Delta T(t')]\mathrm{d}t' \quad [22]$$

where $L(t)$ is the half-diagonal that limits the size and shape of dendritic grains and $v[\Delta T(t')]$ is the growth velocity in the preferential direction. $v[\Delta T(t')]$ can be calculated using the Kurz–Giovanola–Trivedi model.[105] To simulate the nucleation and growth of grains, a time-stepping cellular automaton (CA) was introduced into the R-G model, as shown in Figure 13(a). The predicted grain structure of Al-7 wt pct-Si is presented in Figure 13(b). The advantages of the R-G model include the following: (a) the final computer-predicted microstructures can be directly compared with real microstructures; (b) unlike the finite element method and finite difference method, the R-G model combined with the CA algorithm provides realistic computation times. However, parameters of the 2-D crystal growth and a uniform temperature gradient are needed to achieve accurate solutions. Yao *et al.*[102] proposed a predictive approach named the cellular automaton-finite control volume method (CAFVM) to illustrate the formation and morphology of grains under different conditions, *i.e.*, with and without grain refiners, for Al alloys. Compared with the R-G model, the CAFVM incorporates the solute effect and extra potential nucleants. As a case study, the CAFVM was used to investigate the grain refinement of commercial-purity (CP) Al by Ti. Yao *et al.*'s[102] computed results based on the CAFVM algorithm verified that both nucleants and undercooling ($\geq\Delta T_\mathrm{n}$) play essential roles in grain refinement of CP Al. In addition, Wang *et al.*[106] developed a model to describe grain refinement of single-phase solid-solution alloys based on dendrite fragmentation instead of pure CS-driven nucleation.

VI. NUCLEATION CRYSTALLOGRAPHY OF GRAIN REFINEMENT

The interfacial energy (γ) at the nucleating interface is the controlling factor of heterogeneous nucleation in grain refinement.[32] γ is associated with a few factors,[7,32,45,107] including the chemical and physical nature of nucleant particles, the electrostatic potential between particle and matrix, and the nucleation crystallography across the nucleating interface. Therefore, it is impossible to describe γ using a simple expression. However, Turnbull and Vonnegut theorized that the lattice matching (or structural matching) between

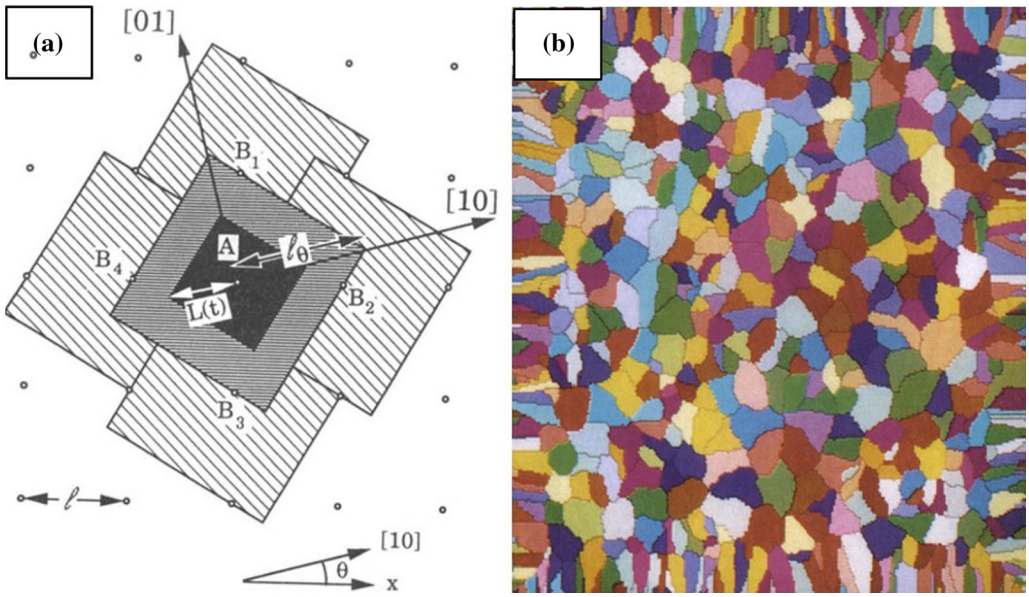

Fig. 13—(*a*) An illustration of the grain-growth of one cellular automaton (CA);[104] (*b*) final grain structure predicted using the two-dimensional CA.[104] (Reprinted with permission from Ref. [104]).

particle and matrix strongly contributes to enhancing heterogeneous nucleation.[108] They predicted that the order of nucleation potency is proportional to the inverse of lattice misfit.[108] Meanwhile, some other investigators have also tried to correlate crystallographic matching (CM) with heterogeneous nucleation.[12,35,48,74,85,86,88,109] Generally, nucleation potency can be evaluated by calculating CM values at the particle/matrix nucleating interface. The better the crystallographic matching, the higher the nucleation potency.[110]

The term nucleation crystallography first appeared in a publication by Qiu and Zhang,[45] followed by Liu *et al.*,[48] on the study of grain refinement of cast Zn. Nucleation crystallography focuses on the role of crystallography between the nucleant particle and metal matrix in grain refinement. Nucleation crystallography addresses crystallographic features like interfacial structure, crystallographic matching, interface orientation, and orientation relationships (ORs).[45] In 1975, Johnson *et al.*[111] had already recognized that when forming a critical nucleus during solid–solid nucleation, the ORs correspond to a facet nucleating interface with low γ. Several representative geometrical models to calculate CM values have been developed, as introduced in Section II–C. Among these models, the E2EM model has proven to be useful for investigating the ORs between the two phases involved in grain refinement.[7,35] A schematic illustration of the E2EM model is provided in Figure 14. The fundamental basis of the E2EM model is that the minimization of γ is likely obtained through appropriate interfacial CM. This model facilitates the study of nucleation crystallography from first principles using crystallographic data; *i.e.*, crystal structure, lattice parameters, and atomic

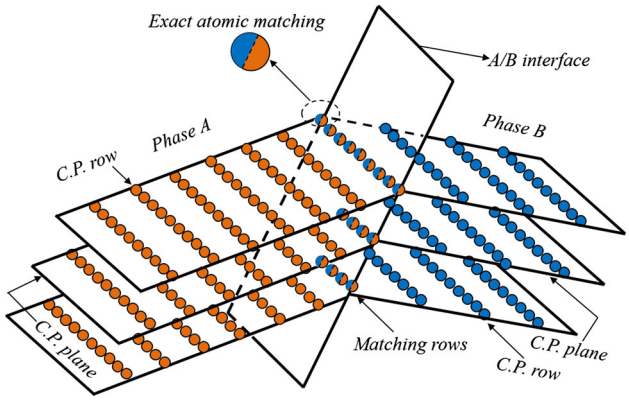

Fig. 14—Schematic illustration of edge-to-edge matching (E2EM) model, indicating evaluation of crystallographic matching based on the interatomic spacing misfit and the interplanar spacing mismatch.

positions. Over the past two decades, the E2EM model has been successfully used to predict nucleant particles for cast metals, such as $Al_3Ti/Al_3Zr/Al_3Nb$ for Al,[12,35,74] $Al_2CO/AlN/Al_2Y/ZnO$ for Mg,[7,86,112,113] $TiB_2/Mg_{24}Y_5$ for β-Li,[88,109] $AgZn_3/CuZn_4/Mg_2Zn$ for Zn,[10,48,98] α-Al_2O_3 for Al_3Ti,[12] and $NbO/CeS/TiN/Ce_2O_3/TiC$ for δ-Fe.[114]

From an atomic perspective, heterogeneous nucleation initiates from atom-by-atom stacking on the naturally exposed crystallographic planes of nucleant particles. Thus, the naturally exposed crystallographic plane serves as the real nucleating plane, rather than the arbitrarily predicted matching planes.[58] It is difficult to control the naturally exposed plane of nucleant particles in grain refinement. The properitectic particles formed *in situ* have a great probability of exposing a favorable

Table III. Crystallographic Matching at the Matrix/Particle Interface in Some Grain Refining Systems That Were Recently Developed

M/P matching(*)	Crystal Structure Information (nm)	OR: $[u\ v\ w]_M$ // $[u'\ v'\ w']_P$, $(h\ k\ l)_M$ // $(h'\ k'\ l')_P$	f_r (pct)(**)	f_d (%)(**)
Mg / Al_2Y[85]	**M**: hcp, $a = 0.3262$, $c = 0.5302$ **P**: fcc, $a = 0.7861$	$[2\bar{1}\bar{1}0]$ // [121], $(0\bar{1}10)$ // $(40\bar{4})$, $(0\bar{1}11)$ // $(3\bar{1}\bar{1})$	0.1	0.1/3.5
Mg / MgO[17]	**M**: hcp, $a = 0.3168$, $c = 0.5235$ **P**: fcc, $a = 0.4234$	$[1\bar{2}10]$ // $[01\bar{1}]$, (0002) // (111)	5.46	6.57
Al / Al_3Nb[74]	**M**: fcc, $a = 0.4049$ **P**: tetragonal, $a = 0.3841$, $c = 0.8609$	[101] // $[02\bar{1}]$, $[0\bar{1}1]$ // [110],$(1\bar{1}\bar{1})$ // $(\bar{1}12)$	0.73/5.43	1.78
Al / Al_3Zr [75]	**M**: fcc, $a = 0.4049$ **P**: tetragonal, $a = 0.4007$, $c = 1.7286$	[101] // $[1\bar{1}0]$,$[1\bar{1}0]$ // $[40\bar{1}]$, $(11\bar{4})$ // $(11\bar{1})$	1.05/1.99	1.34
Zn / $AgZn_3$[48]	**M**: hcp, $a = 0.26649$, $c = 0.49468$ **P**: hcp, $a = 0.28231$, $c = 0.44407$	$[\bar{2}11\bar{3}]$ // $[\bar{1}2\bar{1}0]$, $(10\bar{1}1)$ // $(01\bar{1}1)$, $(10\bar{1}1)$ // (0002)	0.48	2.35/5.81
Zn / Mg_2Zn[98]	**M**: hcp, $a = 0.26649$, $c = 0.49468$ **P**: hcp, $a = 0.5223$, $c = 0.85684$	$[11\bar{2}0]$ // $[\bar{1}\bar{1}20]$, $(1\bar{1}00)$ // (0002), $(000\bar{2})$ // $(1\bar{1}00)$	<6	<10
Li / $Mg_{24}Y_5$[109]	**M**: bcc, $a = 0.351$ **P**: bcc, $a = 1.126$	$[\bar{1}11]$ // [111], (110) // $(3\bar{3}0)$	1.32	6.45
Al_3Ti / α-Al_2O_3[12]	**M**: tetragonal, $a = 0.3846$, c = 0.8594 **P**: trigonal, $a = 0.4759$, c = 1.2991	[110] // $[\bar{1}100]$, $(00\bar{4})$ // $(11\bar{2}\bar{3})$, $(1\bar{1}\bar{2})$ // $(11\bar{2}3)$	6.28	<10
δ-Fe / NbO[114]	**M**: bcc, $a = 0.293$ **P**: fcc, $a = 0.417$	[100] // [110], $(0\bar{2}0)$ // $(2\bar{2}0)$ or $(01\bar{1})$ // $(00\bar{2})$	0.7	0.7/0.7

*M and P refer to matrix and particle.
**f_r and f_d are designated as interatomic misfit and interplanar mismatch, respectively.

crystallographic plane. Preferred ORs often exist in peritectic alloys. After exploring grain refinement of Al by an Al-Ti-B master alloy, Davies *et al.*[115] concluded that properitectic Al_3Ti particles act as the actual nucleation sites and a preferential OR existed between Al_3Ti and Al. Liquid metal atoms stack on the properitectic particles *via* either peritectic reaction or peritectic nucleation.[23,48] This process can be accelerated using an epitaxial atomic configuration. Greninger[116] investigated the OR in a peritectic Cu-Zn alloy system. His X-ray study of the peritectic reaction in a Cu-Zn system confirmed that the ORs are related to the properitectic phase. Marcantonio *et al.*[31] also studied the OR between properitectic particles and a metal matrix using X-rays, finding that the nucleation undercooling increased with lattice misfit (up to 9 pct).

In 1885, Curie[117] proposed that under the equilibrium conditions for the transformation between solid and liquid, crystals will adjust their morphologies to possess minimum surface energies. In other words, the morphology of growing crystals in the equilibrium state should have minimum surface energy. It is well acknowledged that the formation of nuclei will be facilitated if structural matching between particles and nuclei is achieved.[108] Likewise, to minimize the interfacial energy between a solid and liquid, the crystallographic features of a nucleant particle and metal matrix should fulfill the Curie criterion. Close-packed and near-close-packed crystallographic planes are normally considered to satisfy the Curie criterion. For example, Al_3Ti and Zr were found to be potent grain refiners for Al and Mg, respectively. Extensive work on nucleation crystallography has been carried out using the Al/Al_3Ti and Mg/Zr nucleating systems.[56,118] The coherent Kurdjumov–Sachs OR has been observed for the nucleation of β(BCC) on α(FCC) in Cu-Sn alloys[119] and for the nucleation of austenite on primary ferrite in steels.[120] Schaffer *et al.*[118] investigated the role of engulfed and pushed TiB_2 particles in the grain refinement of Al, proving that the ORs with low interfacial energy cause engulfment. In the case of Al-Ti alloys, experiments verified that a preferred OR exists between Al_3Ti and Al.[56]

Normally, the accurate ORs between nucleant particles and a metal matrix can be determined using selected-area electron diffraction (SAED),[45,59] convergent-beam Kikuchi line diffraction (CBKLD),[12,74,75,98,121] or electron backscattering diffraction (EBSD).[48,74,75,112] Transmission electron microscopy (TEM) analysis of the ORs between nucleant particles (TiC) and a metal matrix (α-Al) was performed by Naglić and colleagues.[122] Reference 122 indicated that nucleation occurs on the $\{111\}_{TiC}$ plane so that the $\{111\}_{TiC}$ and $\{111\}_{\alpha-Al}$ planes are in parallel. Cissé *et al.*[123] observed epitaxial growth of α-Al on TiC. The OR between TiC and α-Al is roughly expressed as $[001]_{TiC}//[001]_{\alpha\_Al}$, $(001)_{TiC}//(001)_{\alpha\_Al}$. Using the backscattering electron (BSE) mode in scanning electron microscopy (SEM), Qian *et al.*[124] revealed that effective Zr nucleant particles were surrounded by the Mg matrix. Thereafter, Saha[125] used TEM to accurately determine the ORs between Zr and Mg, which were $(0001)_{Zr}//(0001)_{Mg}$, $(10\bar{1}0)_{Zr}//(10\bar{1}0)_{Mg}$). This suggests that Mg grains were initiated from the basal (0001) plane and prismatic $(10\bar{1}0)$ plane of Zr. Through atom-by-atom stacking, Mg atoms initiated from the $(0001)_{Zr}$ planes of Zr particles during heterogeneous nucleation. The ORs associated with such specific planes ensure a low interfacial energy between nucleant

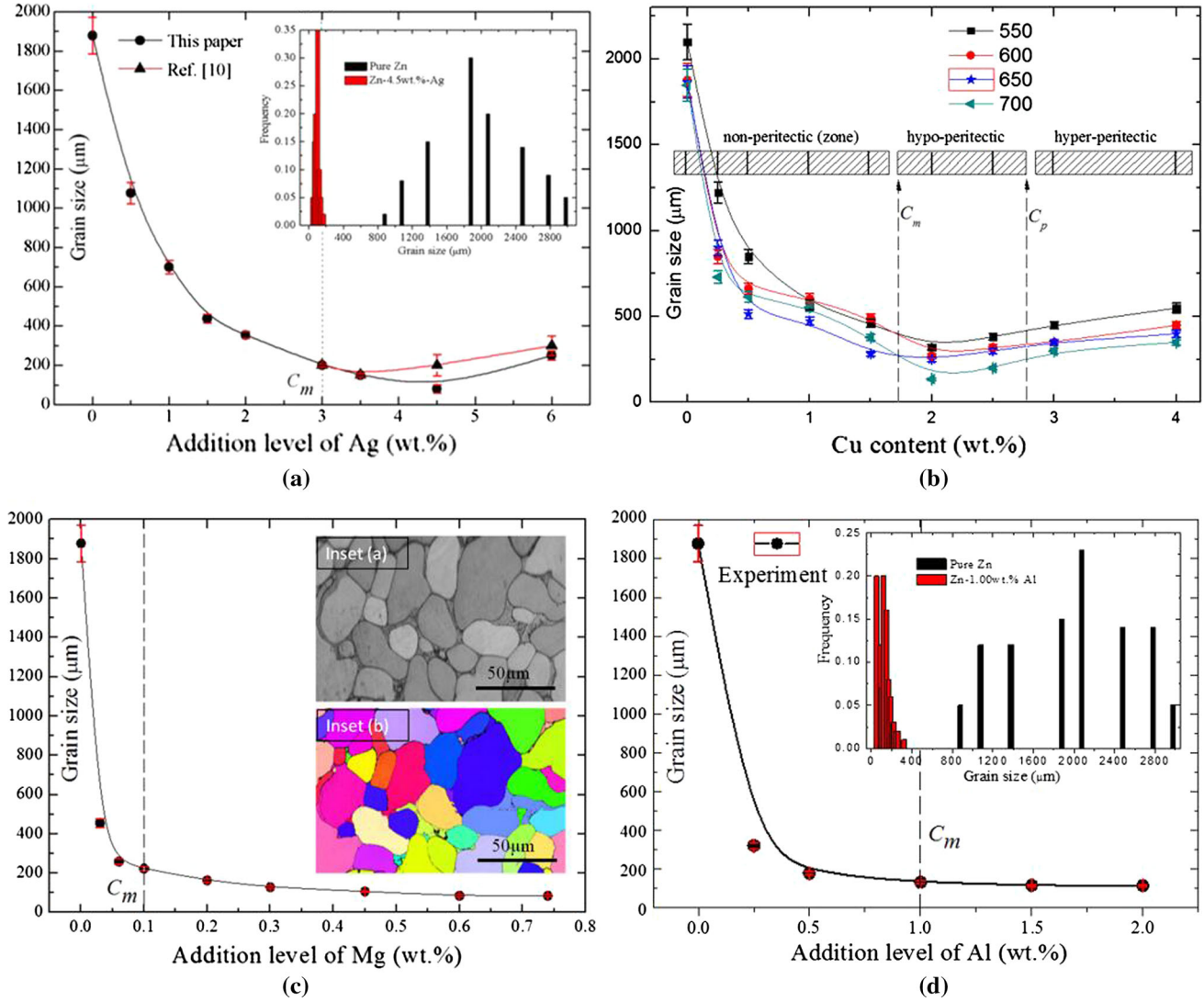

Fig. 15—Cast Zn alloys were grain refined by different grain refiners. The measured grain sizes (*d*) of Zn Alloys plotted against different (*a*) Ag (from Ref. [48]), (*b*) Cu (from Ref. [10]), (*c*) Mg (from Ref. [98]), and (*d*) Al additions (from Ref. [129]). (Reproduced with permissions from the International Union of Crystallography[10] and Ref. [48, 98, 129]).

particles and the metal matrix, resulting in a low nucleation barrier. The crystallographic matching and associated ORs of typical efficient nucleating systems are summarized in Table III. These efficient nucleating systems have been recently used for the grain refinement of Al,[74,75] Mg,[17,85] Zn,[48,98] Li,[109] Al_3Ti,[12] and δ-Fe.[114] Overall, nucleation crystallography can provide guidance to establish a database of effective nucleant particles through crystallographic calculations. Furthermore, a new data-driven approach may be proposed to design grain refiners for specific cast metals/alloys.

VII. GRAIN REFINEMENT OF CAST ZINC AND ITS ALLOYS

The present grain refiners and associated theories/models have mainly focused on light metallic materials, including Al, Mg, Ti, and their alloys. Cast Zn and its alloys have attractive properties such as low melting temperature, high corrosion resistance, and recyclability. As favored engineering materials, they are widely used in transportation, electronics, and mining industries.[27] However, the coarse grains of cast Zn products usually limit their application because they fail to meet the requirements of uniformity, strength, and ductility.[48] There have been few grain refiners developed for cast Zn. Therefore, the grain refinement of cast Zn should be investigated further. Currently, there is little work exclusively on the grain refinement of cast Zn and its alloys. Pollard *et al.*[126] studied the grain refinement of Zn-Al alloys (containing 7 to 24 wt pct Al) by Ti. They attributed the effective grain refinement of α-Al to the presence of some small cubic particles, which served as heterogeneous nucleation sites. Electron probe microanalysis (EPMA) indicated that the cubic particles were actually Al_5Ti_2Zn with $a = 3.99 \pm 0.04$ Å.[126] An approximate calculation showed that the number

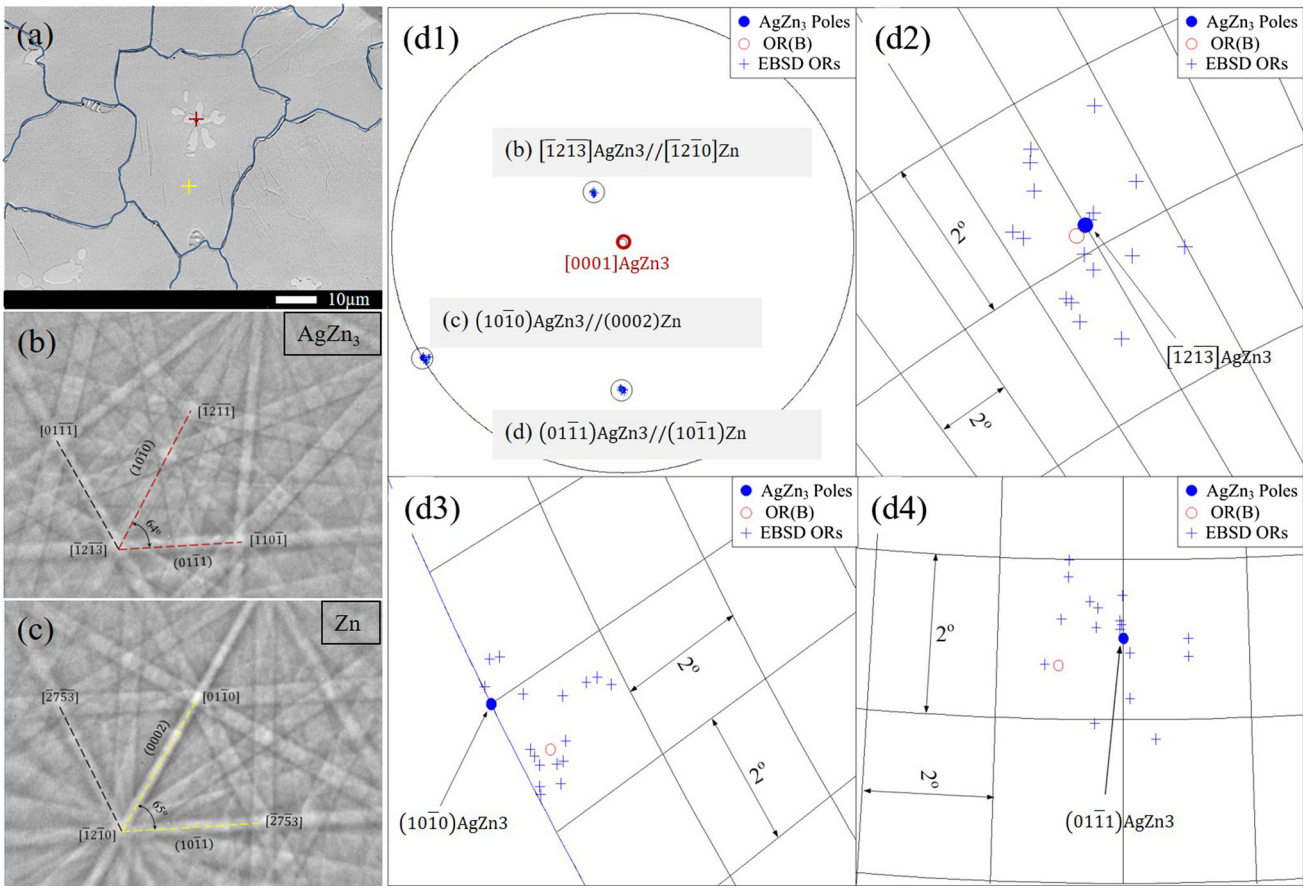

Fig. 16—(*a*) SEM image of one $AgZn_3$/Zn nucleating pair and the corresponding EBSD patterns from (*b*) $AgZn_3$ and (*c*) Zn. (*d*1)–(*d*4) Stereographic projection showing statistical analysis of the experimentally determined OR in (*b*) and (*c*). (Reprinted with permission from Ref. [48]).

density of Al_5Ti_2Zn nucleant particles was of the order of 10^8/cc. In fact, this approach only refines the Al matrix instead of the Zn matrix.

Using thermal analysis, metallography, and EPMA, Leone and co-workers[127] investigated the grain refining mechanism of Zn-Ti and Zn-Ti-Cu alloys. Their experimental results suggested that Zn-Ti-O particles acted as the heterogeneous nucleation sites in the metal melts. Considering the results from EPMA and the available literature, the Zn-Ti-O particles were identified as the spinel oxide Zn_2TiO_4. However, the addition of 1 wt pct Pb into the Zn-Ti-based alloy decreased the grain refining efficiency.[126] It remains unclear why this poisoning phenomenon occurred. Moreover, Kurz and colleagues reported that the Ti-Al-Zn master alloy refined Zn alloys through enhanced heterogeneous nucleation by Al_3Ti/Zn_3Ti.[128] However, these reported grain refiners have low efficacy. Meanwhile, Pb is not environmentally friendly. Therefore, novel potent grain refiners still need to be developed.

Recently, Liu *et al.* carried out a series of systematic investigations on grain refinement of cast Zn and its alloys.[10,27,48,98,99,129] Based on the currently available grain refinement theories/models developed for Al and Mg alloys, four new grain refiners (master alloys) were identified for cast Zn, including Zn-10 wt pct-Ag, Zn-18 wt pct-Cu, Zn-60 wt pct-Mg, and Zn-6 wt pct-Al. Foundry tests showed that these four grain refiners can induce considerable grain refinement in cast Zn, as illustrated in Figure 15. The grain refinement resulting from addition of either Ag (Figure 15(a)) or Cu (Figure 15(b)) is attributed to the cooperative contributions from the segregating solute, which restricts the grain growth, and the properitectic particles formed *in situ*, which enhance heterogeneous nucleation. At high addition levels of solute, formation of coarse properitectic particles decreased the number of active nucleant particles, which are responsible for the grain coarsening of cast Zn alloys.[10,48] The most effective grain refiners used in industry are associated with peritectic-based alloy systems, such as Al-Al_3Nb,[74] Al-Al_3Zr,[75] and Mg-Al_2Y.[85] Specific ORs were reproducibly determined for these peritectic alloys. Similarly, marked grain refinement was found in the peritectic Zn alloys Zn-Ag [48] and Zn-Cu.[10] Ag has a large Q value in liquid Zn. Meanwhile, reproducible ORs were determined in the peritectic Zn/$AgZn_3$ and Zn/$CuZn_4$ nucleating systems. For instance, a new hcp-hcp OR was experimentally determined using EBSD, followed by theoretical validation using the E2EM model. The OR between a Zn metal matrix and $AgZn_3$ nucleant particles is $[\bar{1}2\bar{1}\bar{3}]_{AgZn3}$ // $[\bar{1}2\bar{1}0]_{Zn}$, $(01\bar{1}\bar{1})_{AgZn3}$ // $(10\bar{1}\bar{1})_{Zn}$,

$(10\bar{1}0)_{AgZn3}$ // $(0002)_{Zn}$. Figure 16(a) depicts a BSE micrograph of a $Zn/AgZn_3$ nucleating pair, while Figures 16(b) and (c) show corresponding EBSD patterns. To ensure reproducibility, statistical analysis of this OR was made using stereographic projection, as shown in Figures 16(d1) through (d4). In addition, the eutectic-forming solutes Mg and Al can also considerably refine cast Zn alloys.[98,99,129] $MgZn_2$ particles with a facet morphology were identified to act as heterogeneous nucleation sites. The size distribution of $MgZn_2$ particles lies in a narrow range from 1 to 6 μm. Using CBKLD, an accurate OR between $MgZn_2$ and Zn was measured and expressed as

$$[\bar{1}\bar{1}20]_{MgZn2}\,2.24\text{deg from}\,[11\bar{2}0]_{Zn,}\,(\bar{1}\bar{1}00)_{MgZn2}$$
$$1.12\text{deg from}\,(000\bar{2})_{Zn},\,(0002)_{MgZn2}\,1.8\text{deg from}\,(1\bar{1}00)_{Zn} \quad [23]$$

The efficient grain refinement of cast Zn caused by addition of Mg was concluded to arise from the interdependent contributions from (a) the growth restriction effect of Mg as a powerful segregating solute, (b) the $MgZn_2$-enhanced heterogeneous nucleation, and (c) the suitable geometrical features of the $MgZn_2$ nucleant particles.[98] The reason why Al leads to remarkable grain refinement is being investigated in detail. Additionally, larger errors arise when evaluating the Q values of Zn alloys with higher solute content. This is attributed to the deviation from a linear dependence on c_o at higher solute content.[60] Therefore, a new method for quantitative calculation of the Q values of multiple-component Zn alloys in which strong solute–solute interaction occurs is required.

VIII. CONCLUSIONS AND FUTURE WORK

Based on this review, a few important conclusions can be made to guide the design of effective grain refiners (or master alloys) for cast metals/alloys. (a) Enough potent nucleant particles are needed for heterogeneous nucleation. Normally, these nucleant particles (native or formed *in situ*) should have a crystallographic relationship with their counterpart metal matrix. In peritectic-based alloys, the properitectic particles usually ensure that this crystallographic requirement is met. (b) Nucleant particles should possess suitable geometrical features, including particle size, size distribution, and morphology. (c) Grain refiners need to contain powerful segregating solute elements that have high Q values in the liquid metal. Such solute elements can provide a large thermodynamic driving force for nucleation in grain refinement. Future studies on grain refinement of cast metals/alloys may focus on the issues below that involve grain nucleation and growth.

(i) Heterogeneous nucleation starts from atom-by-atom stacking on the naturally exposed crystallographic plane of nucleant particles. These metallic atoms come from the liquid metal surrounding nucleant particles. It is important to determine how the solute atoms influence the crystallographic matching at the nucleating interface. This issue will be closely associated with the nucleant selection and nucleation barrier.

(ii) Currently, the growth restriction factor (Q value) is mainly used in binary refining alloy systems, such as Al, Mg, Ti, and Zn alloys. However, the accurate calculation of Q values for multiple-component alloys still remains a challenge. Novel thermodynamic calculation methods may reveal how to minimize the NFZ by controlling alloy chemistry and/or growth rate. Furthermore, both particle efficacy and grain refinement may be improved.

(iii) Quantifying the effect of different solutes on the ΔG for nucleation in grain refinement. It has been recognized that peritectic-forming solute elements produce larger ΔG values than the eutectic-forming solute elements in a given alloy system. However, this situation may be not applicable in other alloy systems, such as Zn alloys. Thus, more quantitative calculation of ΔG values should be carried out for other alloys, *i.e.*, Mg, Ti, Fe, Cu, and Zn, to verify this phenomenon.

(iv) Real castings form in a 3-D metal melt scenario. To accurately interpret the nucleation and growth of grains in grain refinement, it is probably best to incorporate CS-related models into simulations (such as the phase field method), followed by real-time experimental investigation using synchrotron radiation or other techniques.

(v) From a geometrical perspective, what is the optimal size range of nucleant particles available for CS-driven nucleation? This size range can be controlled to enhance the heterogeneous nucleation on potent particles, further promoting grain refinement. Modeling on such a topic should consider the growth velocity, solute diffusion, interfacial energy, fusion entropy, and Q value. Both deterministic and probabilistic modeling ought to be combined in these investigations.

(vi) Recently, large-scale castings have been paid much attention. Grain refinement of large-scale castings has seldom been reported. Current theories/models of grain refinement were mainly developed for small-scale castings. It is currently unclear if these theories/models can be fully applied to large-scale castings. Advances in research on grain refinement of large-scale castings are required.

ACKNOWLEDGMENTS

Sincere appreciation is expressed to Professor Mingxing Zhang, A/Professor John A. Taylor, and Emeritus Professor David StJohn at The University of Queensland (UQ), Dr. Dong Qiu and Professor Mark A. Easton at RMIT University, and Dr. Feng Wang at Brunel University London for their engaged discussion

when I studied at UQ. This work is supported by National Natural Science Foundation of China (Grant No. 51605496), and also financially funded by the State Key Laboratory of High Performance Complex Manufacturing (No. ZZYJKT2016-03). Zhilin Liu would like to acknowledge Jing Ouyang (his wife) for her love, understanding and support during this work.

REFERENCES

1. A.L. Greer, P.S. Cooper, M.W. Meredith, W. Schneider, P. Schumacher, J.A. Spittle, and A. Tronche: *Adv. Eng. Mater.*, 2003, vol. 5, pp. 81–91.
2. D.H. StJohn, M. Qian, M.A. Easton, and P. Cao: *Acta Mater.*, 2011, vol. 59, pp. 4907–21.
3. B.S. Murty, S.A. Kori, and M. Chakraborty: *Int. Mater. Rev.*, 2002, vol. 47, pp. 3–29.
4. A. Cibula: *J. Institute Metals*, 1949–1950, vol. 76, pp. 321–60.
5. D.M. Stefanescu: *Science and engineering of casting solidification*, Kluwer Academic/Plenum Publisher, New York, 2002.
6. A.L. Greer, A.M. Bunn, A. Tronche, P.V. Evans, and D.J. Bristow: *Acta Mater.*, 2000, vol. 48, pp. 2823–35.
7. M.X. Zhang, P.M. Kelly, M. Qian, and J.A. Taylor: *Acta Mater.*, 2005, vol. 53, pp. 3261–70.
8. I. Polmear, D.H. StJohn, J.F. Nie, and M. Qian: *Light Alloys: Metallurgy of the Light Alloys*, 5th ed., Butterworth-Heinemann, 2017.
9. P. Cao, M. Qian, and D.H. StJohn: *Scripta Mater.*, 2005, vol. 53, pp. 841–44.
10. Z.L. Liu, D. Qiu, F. Wang, J.A. Taylor, and M.X. Zhang: *J. Appl. Cryst.*, 2015, vol. 48, pp. 890–900.
11. D. Qiu and M.X. Zhang: *J. Alloys Compd.*, 2009, vol. 488, pp. 260–64.
12. F. Wang, D.G. Eskin, J.W. Mi, and M. Mounib: *Acta Mater.*, 2016, vol. 116, pp. 354–63.
13. M.A. Easton and D.H. StJohn: *Metall. Mater. Trans. A*, 1999, vol. 30, pp. 1613–23.
14. P. de Gennes: *Rev. Mod. Phys.*, 1985, vol. 57, pp. 827–63.
15. D.A. Porter and K.E. Eastering: *Phase Transformatios in Metals and Alloys*, CRC Press, Boca Raton, 1992.
16. M.E. Glicksman: *Principles of Solidification: An Introduction to Modern Casting and Crystal Growth Concept*, Springer, New York, 2011.
17. Z. Fan, Y. Wang, M. Xia, and S. Arumuganathar: *Acta Mater.*, 2009, vol. 57, pp. 4891–4901.
18. M. Johnsson, L. Backerud, and G. Sigworth: *Metall. Mater. Trans. A*, 1993, vol. 24 (2), pp. 481–91.
19. F. Wang, Z.L. Liu, D. Qiu, J.A. Taylor, M.A. Easton, and M.X. Zhang: *Metall. Mater. Trans. A*, 2015, vol. 46A, pp. 505–15.
20. M. Johnsson: *Thermochimica Acta*, 1995, vol. 256, pp. 107–21.
21. W. Kurz and J. Fisher: *Fundamentals of solidification*, Transaction and Technology Publications, Brookfield, 1989.
22. M. Rappaz: *Int. Mater. Rev.*, 1989, vol. 34, pp. 93–124.
23. F. Wang, Z.L. Liu, D. Qiu, J.A. Taylor, M.A. Easton, and M.X. Zhang: *Acta Mater.*, 2013, vol. 61, pp. 360–70.
24. Y. Lee, A. Dahle, and D.H. StJohn: *Metall. Mater. Trans. A*, 2000, vol. 31A, pp. 2895–2906.
25. S. Tamirisakandala, R.B. Bhat, J.S. Tiley, and D.B. Miracle: *Scripta Mater.*, 2005, vol. 53, pp. 1421–26.
26. M.J. Balart, J.B. Patel, F. Gao, and Z. Fan: *Metall. Mater. Trans. A*, 2016, vol. 47, pp. 4988–5011.
27. Z.L. Liu, F. Wang, D. Qiu, J.A. Taylor, and M.X. Zhang: *Metall. Mater. Trans. A*, 2013, vol. 44, pp. 4025–30.
28. N. Iqbal: *Real-Time Investigation of Grain Nucleation and Growth During Liquid to Solid Phase Transformation of Aluminum Alloys*, PhD thesis, Delft University of Technology, The Netherlands, 2005.
29. M.E. Glicksman and W.J. Childs: *Acta Metall.*, 1962, vol. 10, pp. 925–33.
30. T. Skaland: *Proceeding of the AFS Cast Iron Inoculation Conference*, 2005.
31. J. Marcantonio and L.F. Mondolfo: *J. Inst. Metals*, 1970, vol. 98, pp. 23–27.
32. B. Bramfitt: *Metall. Mater. Trans. B*, 1970, vol. 1, pp. 1987–95.
33. L.F. Mondolfo, B. Vonnegut, and H. Chessin: *Science*, 1972, vol. 176, pp. 695–96.
34. D. Turnbull: *Acta Metall.*, 1953, vo. 1, pp. 7–10.
35. M.X. Zhang, P.M. Kelly, M.A. Easton, and J.A. Taylor: *Acta Mater.*, 2005, vol. 53, pp. 1427–38.
36. Y. Ali, D. Qiu, B. Jiang, F. Pan, and M.X. Zhang: *J. Alloys Compd.*, 2015, vol. 619, pp. 639–51.
37. I. Maxwell and A. Hellawell: *Acta Metall.*, 1975, vol. 23, pp. 229–37.
38. T.E. Quested and A.L. Greer: *Acta Mater.*, 2004, vol. 52, pp. 3859–68.
39. A.L. Greer: *Phil. Trans. Royal Soc. A-Math. Phy. Eng. Sci.*, 2003, vol. 361, pp. 479–94.
40. M. Qian, D.H. StJohn, and M.T. Frost: *Scripta Mater.*, 2004, vol. 50, pp. 1115–19.
41. J.H. Perepezko: *Metals Handbook*, ASM, New York, Metals Park, 1988.
42. M.A. Easton and D.H. StJohn: *Mater. Sci. Eng. A*, 2008, vol. 486, pp. 8–13.
43. Y. Zhang, H. Zheng, Y. Liu, L. Shi, R. Xu, and X. Tian: *Acta Mater.*, 2014, vol. 70, pp. 162–73.
44. M. Lazaridis, M. Kulmala, and B.Z. Gorbunov: *J. Aer. Sci.*, 1992, vol. 23, pp. 457–66.
45. D. Qiu and M.X. Zhang: *J. Alloy Compd.*, 2013, vol. 586, pp. 39–44.
46. W.B. Li and K.E. Easterling: *Acta Metall. Mater.*, 1990, vol. 38, pp. 1045–52.
47. M. Qian: *Acta Mater.*, 2007, vol. 55, pp. 943–53.
48. Z.L. Liu, D. Qiu, F. Wang, J.A. Taylor, and M.X. Zhang: *Acta Mater.*, 2014, vol. 79, pp. 315–26.
49. S.E. Offerman, N.H. van Dijk, J. Sietsma, S. Grigull, E.M. Lauridsen, L. Margulies, H.F. Poulsen, M.T. Rekveldt, and S. van der Zwaag: *Science*, 2002, vol. 298, pp. 1003–05.
50. D.A. Porter, K.E. Easterling, and M.Y. Sherif: *Phase Transformation in Metals and Alloys*, Taylor & Francis, London, 2009.
51. W.J. Jakson: *Iron and Steel*, 1972, vol. 45, pp. 163–72.
52. M.J. Bermingham, S.D. McDonald, M.S. Dargusch, and D.H. StJohn: *Scripta Mater.*, 2008, vol. 58, pp. 1050–53.
53. N.H. Fletcher: *J. Chem. Phy.*, 1958, vol. 29, pp. 572–76.
54. B. Cantor: *Phil. Trans. Royal Soc. A-Math. Phy. Eng. Sci.*, 2003, vol. 361, pp. 409–16.
55. B. Chalmers: *Principles of Solidification*, John Viley, New York, 1964, pp. 77–83.
56. P. Schumacher, A.L. Greer, J. Worth, P.V. Evans, M.A. Kearns, P. Fisher, and A.H. Green: *Mater. Sci. Tech.*, 1998, vol. 14, pp. 394–404.
57. J.H. Li, M.Z. Zarif, M. Albu, B.J. McKay, F. Hofer, and P. Schumacher: *Acta Mater.*, 2014, vol. 72, pp. 80–98.
58. Z. Fan: *Metall. Mater. Trans. A*, 2013, vol. 44A, pp. 1409–18.
59. Z. Fan, Y. Wang, Y. Zhang, T. Qin, X.R. Zhou, G.E. Thompson, T. Pennycook, and T. Hashimoto: *Acta Mater.*, 2015, vol. 84, pp. 292–304.
60. T.E. Quested, A.T. Dinsdate, and A.L. Greer: *Acta Mater.*, 2005, vol. 53, pp. 1323–34.
61. A. Hellawell: *Heterogeneous Nucleation and Grain Refinement in Aluminium Castings*, Solidification and Casting of Metals (Conference), London, 1977, pp. 161–68.
62. I.G. Davies, J.M. Dennis, and A. Hellawell: *Metall. Trans.*, 1970, vol. 1 (1), pp. 275–80.
63. M.A. Easton and D.H. StJohn: *Acta Mater.*, 2001, vol. 49, pp. 1867–78.
64. R. Günther, C. Hartig, and R. Bormann: *Acta Mater.*, 2006, vol. 54, pp. 5591–97.
65. H. Men and Z. Fan: *Acta Mater.*, 2011, vol. 59, pp. 2704–12.
66. M. Abdel-Reihim, N. Hess, W. Reif, and M.E.J. Birch: *J. Mater. Sci.*, 1987, vol. 22, pp. 213–18.
67. W.A. Tiller, K.A. Jackson, J.W. Rutter, and B. Chalmers: *Acta Metall.*, 1953, vol. 1, pp. 428–37.
68. T.T. Cheng: *Intermetallics*, 2000, vol. 8, pp. 29–37.
69. M.C. Flemings: *Metall. Trans.*, 1974, vol. 5, pp. 2121–34.
70. M. Xu, L. Fabietti, Y. Song, D. Tourret, A. Karma, and R. Trivedi: *Scripta Mater.*, 2014, vol. 88, pp. 29–32.

71. D.H. StJohn, A. Prasad, M.A. Easton, and M. Qian: *Metall. Mater. Trans. A*, 2015, vol. 46A, pp. 4868–85.
72. T. Izumi, Y. Nakamura, and Y. Shiohara: *J. Cryst. Growth*, 1993, vol. 128, pp. 757–61.
73. F.A. Crossley and L.F. Mondolfo: *J. Metals (New York)*, 1951, vol. 3, pp. 1143–50.
74. F. Wang, D. Qiu, Z.L. Liu, J.A. Taylor, M.A. Easton, and M.X. Zhang: *J. Appl. Cryst.*, 2014, vol. 47, pp. 770–79.
75. F. Wang, D. Qiu, Z.L. Liu, J.A. Taylor, M.A. Easton, and M.X. Zhang: *Acta Mater.*, 2013, vol. 61, pp. 5636–45.
76. E.F. Emley: *Principles of magnesium technology*, Pergamon Press, Oxford, 1966.
77. M. Qian and A. Das: *Scripta Mater.*, 2006, vol. 54, pp. 881–86.
78. L. Backerud and Y. Shao: *Aluminium (Germany)*, 1991, vol. 67, pp. 780–85.
79. C.D. Mayes, D.G. McCartney, and G.J. Tatlock: *Mater. Sci. Tech.*, 1993, vol. 9, pp. 97–103.
80. P.S. Mohanty and J.E. Gruzleski: *Acta Metall. Mater.*, 1995, vol. 43, pp. 2001–12.
81. G. Jones and J. Pearson: *Metall. Mater. Trans. B*, 1976, vol. 7, pp. 223–34.
82. P. Cao, M. Qian, and D.H. StJohn: *Scripta Mater.*, 2005, vol. 53, pp. 841–44.
83. M.A. Easton, A. Schiffl, J.Y. Yao, and H. Kaufmann: *Scripta Mater.*, 2006, vol. 55, pp. 379–82.
84. Y. Liu, X. Liu, and B. Xiufang: *Mater. Lett.*, 2004, vol. 58, pp. 1282–87.
85. D. Qiu, M.X. Zhang, J.A. Taylor, and P.M. Kelly: *Acta Mater.*, 2009, vol. 57, pp. 3052–59.
86. H.M. Fu, M.X. Zhang, D. Qiu, P.M. Kelly, and J.A. Taylor: *J. Alloys Compd.*, 2009, vol. 478, pp. 809–12.
87. P. Cao, M. Qian, D.H. StJohn: *Scripta Mater.*, 2004, vo. 51, pp. 125-29.
88. B. Jiang, D. Qiu, M.X. Zhang, P.D. Ding, and L. Gao: *J. Alloys Compd.*, 2010, vol. 492, pp. 95–98.
89. M.A. Easton, M. Qian, A. Prasad, and D.H. StJohn: *Curr. Opin. Solid State Mater. Sci.*, 2016, vol. 20 (1), pp. 13–24.
90. M.J. Bermingham, S.D. McDonald, K. Nogita, D.H. StJohn, and M.S. Dargusch: *Scripta Mater.*, 2008, vol. 59, pp. 538–41.
91. M.J. Bermingham, S.D. McDonald, D.H. StJohn, and M.S. Dargusch: *J. Alloys Compd.*, 2009, vol. 481, pp. 20–23.
92. B. Chalmers: *Trans. Am. Soc. Met.*, 1954, vol. 46, pp. 1214–24.
93. G. Chai, L. Bäckerud, T. Rølland, and L. Arnberg: *Metall. Mater. Trans. A*, 1954, vol. 26 (4), pp. 965–70.
94. M.A. Easton and D.H. StJohn: *Metall. Mater. Trans. A*, 2005, vol. 36, pp. 1911–20.
95. D.H. StJohn, M. Qian, M.A. Easton, P. Cao, and Z. Hildebrand: *Metall. Mater. Trans. A*, 2005, vol. 36, pp. 1669–79.
96. M. Qian, P. Cao, M.A. Easton, S.D. McDonald, and D.H. StJohn: *Acta Mater.*, 2010, vol. 58, pp. 3262–70.
97. Y. Chen, S. Zhang, H. Song, M. Cheng, H. Li, and J. Liu: *Materials & Design*, 2016, vol. 91, pp. 314–20.
98. Z.L. Liu, D. Qiu, F. Wang, J.A. Taylor, and M.X. Zhang: *Mater. Charact.*, 2015, vol. 106, pp. 1–10.
99. Z.L. Liu, R.Q. Li, R.P. Jiang, X.Q Li, and M.X. Zhang: *J. Alloy Compd.*, 2016, vol. 687, pp. 885–92.
100. M.A. Martorano and V.B. Biscuola: *Acta Mater.*, 2009, vol. 57, pp. 607–15.
101. L. Nastac and D. Stefanescu: *Metall. Trans. A*, 1993, vol. 24, pp. 2107–18.
102. X. Yao, S.D. McDonald, A.K. Dahle, C.J. Davidson, and D.H. StJohn: *J. Mater. Res.*, 2008, vol. 23, pp. 1282–91.
103. J.D. Hunt: *Mater. Sci. Eng.*, 1985, vol. 65, pp. 75–83.
104. M. Rappaz and C.A. Gandin: *Acta Metall. Mater.*, 1993, vol. 41, pp. 345–60.
105. W. Kurz, B. Giovanola, and R. Trivedi: *Acta Metall.*, 1986, vol. 34, pp. 823–30.
106. H. Wang, F. Liu, and Y. Tan: *Acta Mater.*, 2011, vol. 59, pp. 4787–97.
107. X. Cao and J. Campbell: *Metall. Mater. Trans. A*, 2003, vol. 34, pp. 1409–20.
108. D. Turnbull and B. Vonnegut: *Ind. Eng. Chem.*, 1952, vol. 44 (6), pp. 1292–98.
109. Y. Zeng, B. Jiang, M.X. Zhang, H. Yin, R. Li, and F. Pan: *Intermetallics*, 2014, vol. 45, pp. 18–23.
110. H.T. Li, Y. Wang, and Z. Fan: *Acta Mater.*, 2012, vol. 60, pp. 1528–37.
111. W.C. Johnson, C.L. White, P.E. Marth, P.K. Ruf, S.M. Tuominen, K.D. Wade, K.C. Russell, and H.I. Aaronson: *Metall. Trans. A*, 1975, vol. 6, pp. 911–19.
112. D. Qiu, M.X. Zhang, and P.M. Kelly: *Scripta Mater.*, 2009, vol. 61, pp. 312–15.
113. H.M. Fu, D. Qiu, M.X. Zhang, H. Wang, P.M. Kelly, and J.A. Taylor: *J. Alloys Compd.*, 2008, vol. 456, pp. 390–94.
114. M. Li, J.M. Li, D. Qiu, Q. Zhang, G. Wang, and M.X. Zhang: *Philos. Mag.*, 2016, vol. 96, pp. 1556–78.
115. I. Davies, J. Dennis, and A. Hellawell: *Metall. Mater. Trans. B*, 1970, vol. 1, pp. 275–80.
116. A.B. Greninger: *Nature*, 1936, vol. 2, pp. 657–58.
117. P. Curie: *Bull. Soc. min. de France*, 1885, vol. 8, p. 145.
118. P.L. Schaffer, D.N. Miller, and A.K. Dahle: *Scripta Mater.*, 2007, vol. 57, pp. 1129–32.
119. A. Banerji, Q. Feng, and W. Reif: *Metall. Mater. Trans. A*, 1989, vol. 20, pp. 564–66.
120. G. Thewlis, J.A. Whiteman, and D.J. Senogles: *Mater. Sci. Tech.*, 1997, vol. 13, pp. 257–74.
121. M.X. Zhang and P.M. Kelly: *Prog. Mater. Sci.*, 2009, vol. 54, pp. 1101–70.
122. A.S.I. Naglić and M. Dobersek: *Metallic Materials*, 2007, vol. 45, pp. 293–99.
123. J. Cissé, G.F. Bolling, and H.W. Kerr: *J. Cryst. Growth*, 1972, vols. 13–14, pp. 777–81.
124. M. Qian and D.H. StJohn: *Int. J. Cast Metal Res.*, 2009, vol. 22 (1–4), pp. 256–59.
125. P. Saha: *An analysis of the grain refinement of magnesium by zirconium*, PhD thesis, The University of Alabama, Alabama, 2010.
126. W.A. Pollard, K.M. Pickwick, J.T. Jubb, and R.H. Packwood: *Can. Metall. Q.*, 1974, vol. 13, pp. 535–43.
127. G. Leone, P. Niessen, and H. Kerr: *Metall. Mater. Trans. B*, 1975, vol. 6, pp. 503–11.
128. W. Kurz, B. Giovanola, and R. Trivedi: *Acta Metall.*, 1986, vol. 34 (5), pp. 823–30.
129. Z.L. Liu, D. Qiu, F. Wang, J.A. Taylor, and M.X. Zhang: *Metall. Mater. Trans. A*, 2016, vol. 47 (2), pp. 830–41.